ECOM-74-0470-2

SYSTEMATIC STUDY OF PYROELECTRICITY

Generalized Molecular Field Theory of Ferroelectricity and Pyroelectricity

M.I. Bell and P.M. Raccah
Yeshiva University
Belfer Graduate School of Science
Amsterdam Ave., 186th St.
New York, NY 10033

October 1975

Interim Report for Period 1 October 1974 - 31 March 1975

Approved for public release; distribution unlimited

Sponsored by

ADVANCED RESEARCH PROJECTS AGENCY
1400 Wilson Blvd.
Arlington, VA 22209
ARPA Order No. 2573

US Army Electronics Command
Fort Monmouth, NJ 07703

NOTICES

Disclaimers

The findings in this report are not to be construed as an official Department of the Army position, unless so designated by other authorized documents.

The citation of trade names and names of manufacturers in this report is not to be construed as official Government indorsement or approval of commercial products or services referenced herein.

Disposition

Destroy this report when it is no longer needed. Do not return it to the originator.

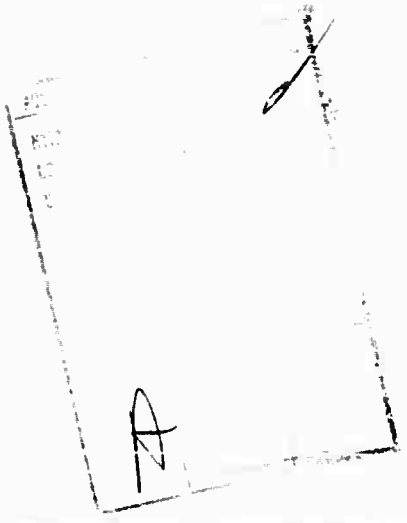

ESC-FM 5700-65

UNCLASSIFIED
SECURITY CLASSIFICATION OF THIS PAGE (When Data Entered)

REPORT DOCUMENTATION PAGE

READ INSTRUCTIONS BEFORE COMPLETING FORM

1. REPORT NUMBER: ECOM-74-0470-2
2. GOVT ACCESSION NO.
3. RECIPIENT'S CATALOG NUMBER
4. TITLE (and Subtitle): SYSTEMATIC STUDY OF PYROELECTRICITY. Generalized Molecular Field Theory of Ferroelectricity and Pyroelectricity
5. TYPE OF REPORT & PERIOD COVERED: Semiannual Technical Report, 1 Oct 74 — 31 Mar 75
6. PERFORMING ORG. REPORT NUMBER
7. AUTHOR(s): M.I. Bell and P.M. Raccah
8. CONTRACT OR GRANT NUMBER(s): DAAB 07-74-C-0470, ARPA Order-2573
9. PERFORMING ORGANIZATION NAME AND ADDRESS: Yeshiva University, Belfer Graduate School of Science - 2495 Amsterdam Ave, New York, NY 10033
10. PROGRAM ELEMENT, PROJECT, TASK AREA & WORK UNIT NUMBERS: Program Code No. 4010
11. CONTROLLING OFFICE NAME AND ADDRESS: Advanced Research Projects Agency, 1400 Wilson Blvd., Arlington, VA 22209
12. REPORT DATE: October 1975
13. NUMBER OF PAGES: 49 (54p.)
14. MONITORING AGENCY NAME & ADDRESS (if different from Controlling Office): US Army Electronics Command, Fort Monmouth, NJ 07703 AMSEL-TL-ES
15. SECURITY CLASS. (of this report): Unclassified
15a. DECLASSIFICATION/DOWNGRADING SCHEDULE

16. DISTRIBUTION STATEMENT (of this Report)

Approved for public release; distribution unlimited

17. DISTRIBUTION STATEMENT (of the abstract entered in Block 20, if different from Report)

18. SUPPLEMENTARY NOTES

This research was supported by Advanced Research Projects Agency of the Department of Defense and was monitored by US Army Electronics Command under Contract No. DAAB-07-74-C-0470 (see reverse side)

19. KEY WORDS (Continue on reverse side if necessary and identify by block number)

Ferroelectrics, Pyroelectric detectors, Figure of merit, Phase transitions, Molecular field theory, Triglycine sulfate.

20. ABSTRACT (Continue on reverse side if necessary and identify by block number)

The generalized molecular field theory of ferroelectricity developed previously by the authors is used to obtain exact expressions for the ferroelectric properties of crystals (spontaneous polarization, dielectric susceptibility, critical temperature and polarization) and for the resulting pyroelectric properties (pyroelectric coefficient and response figure of merit for radiation detection). Good agreement between theory and experiment is found for the spontaneous polarization of triglycine sulfate. The response figure of merit is found to exhibit an interesting

over

DD FORM 1 JAN 73 1473 EDITION OF 1 NOV 65 IS OBSOLETE

UNCLASSIFIED
SECURITY CLASSIFICATION OF THIS PAGE (When Data Entered)

053 820

18. Supplementary Notes (cont'd)

Effective date of Contract - 1 October 1973

Amount of Contract - Total amount: $148,840
First year: $ 72,582
Second year: $ 76,258

ARPA Contractor: Yeshiva University
P.M. Raccah, Principal Investigator
(212) 568-8400

Project Scientists: FREDERICK ROTHWARF, (201) 544-4407
GERALD J. IAFRATE (201) 544-4070

20. Abstract (cont'd)

universal behavior which may prove useful in optimizing detector performance. The well-known Devonshire formalism, obtained by truncating the power-series expansion for the free energy, is found to yield a relatively poor approximation to the results of the generalized molecular field theory.

CONTENTS

I. INTRODUCTION

The work described in this report was conducted from 1 October 1974 to 31 March 1975 under Advanced Research Projects Agency Contract DAAB 07-74-C-0470, P.M. Raccah, principal investigator, F. Rothwarf, and G. Iafrate, contract monitors. The purpose of this investigation is to elucidate the physical mechanism responsible for the pyroelectric effect in ferroelectric crystals. We have proposed a generalized molecular field theory (GMFT) of ferroelectricity and pyroelectricity[1,2] which yields good agreement with the available experimental data for $BaTiO_3$. Unfortunately, these results are limited in two respects. First, only $BaTiO_3$ has been studied in sufficient detail to provide the input data needed for our theory, and second, the calculations reported previously are approximate ones, valid only when the polarization is near zero or near its saturation value. We present here exact calculations based on the generalized molecular field theory[1] which remove the restrictions on the magnitude of the polarization. These were undertaken both to explore the detailed behavior of the GMFT and to provide a framework for the analysis of measurements currently in progress on a number of materials in order to obtain input data for the theory. The experiments will be described in a forthcoming report.

After a brief summary of the GMFT and the introduction of reduced (dimensionless) variables which greatly simplify the calculations (Section II), we present in Section III exact calculations of the static properties of our model (spontaneous polarization, critical temperature, critical polarization). Then Section IV gives exact results for the dynamic properties: susceptibility, pyroelectric coefficient, and response figure of merit for pyroelectric detection. Throughout, we treat both the case of a local field expressed as a power series in the polarization and that of the field

represented by a Padé approximant[1]. We also compare the exact results with those obtained from an approximate free energy of the type proposed by Devonshire[3].

An important result of the present study (Section IV) is that the GMFT predicts that the response figure of merit of a pyroelectric detector M_1, which is the ratio of the pyroelectric coefficient and the dielectric constant, will exhibit an interesting, and potentially useful, universal behavior. When expressed in terms of reduced variables, this figure of merit depends only on the spontaneous polarization, indicating that M_1 should be regarded as a function of polarization rather than temperature when trends or systematic variations between materials are being sought. Work is now in progress to exploit this fact as a tool for optimizing M_1.

Finally, Section V presents a preliminary fit of the observed temperature dependence of the spontaneous polarization of triglycine sulfate to the prediction of the GMFT. Good agreement is obtained by trial-and-error adjustment of GMFT parameters, and a computer program is now being written to obtain the best fit (in the sense of mean-square deviation) and so determine the GMFT parameters with the greatest precision compatible with the accuracy of the experimental data.

II. SUMMARY OF GMFT

As is well known, molecular field theory predicts that a system of N independent electric dipoles of moment $\vec{\mu}$ which can assume any orientation in space will exhibit a macroscopic polarization $\vec{P}$ at temperature T given by

$$P = N\mu \, (\coth x - 1/x) \, , \tag{1}$$

where

$$x = \mu E_\ell / kT \, , \tag{2}$$

E_ℓ is the local electric field at the site of each dipole, and k is Boltzmann's constant. The usual Weiss molecular field theory results from the assumption that the local field has the Lorentz form:

$$E_\ell = E + \lambda P \, , \tag{3}$$

where E is the applied field and λ is a constant. The GMFT is obtained[1] when one replaces the linear Lorentz correction λP by an internal field containing higher powers of P:

$$E_\ell = E + \lambda P + \lambda' P^3 + \lambda'' P^5 + \ldots \tag{4}$$

As we have noted elsewhere[1,2], this form for the local field is closely related to that introduced by Onsager[4] in treating polar fluids. It is readily shown[1] that Eqs. (1), (2), and (4) lead to a free energy of the form

$$G = \tfrac{1}{2} A_o (T-T_o) \, P^2 + \tfrac{1}{4} B_o (T-T_1) \, P^4 + \tfrac{1}{6} C_o (T-T_2) \, P^6 + \ldots \, , \tag{5}$$

where

$$A_o = 3k/N\mu^2 \qquad T_o = \lambda/A_o$$

$$B_o = 3A_o/5\ (N\mu)^2 \qquad T_1 = \lambda'/B_o \tag{6}$$

$$C_o = 99\ A_o/175(N\mu)^4 \qquad T_2 = \lambda''/C_o$$

and so forth. The field E and susceptibility χ are obtained from G by differentiation:

$$E = \partial G/\partial P \tag{7}$$

and

$$1/\chi = \partial E/\partial P = \partial^2 G/\partial P^2 \ . \tag{8}$$

The feature of the free energy (5) which is unusual for a molecular field theory is that the system may enter a spontaneously polarized state via a phase transition which is either second order (for $T_1 < T_o$, occurring at $T = T_o$) or first order (for $T_1 > T_o$, occurring at $T = T_c > T_o$).

If the power series (4) is regarded as only an approximation for E_ℓ, it is reasonable to examine other functional forms which yield (4) for small values of P. One such form, obtained from the theory of Padé approximants, is[1]

$$E_i = E + \frac{\lambda P}{1-(\lambda'/\lambda)P^2} \ . \tag{9}$$

Since this form predicts λ' in good agreement[1] with the value deduced from experiment in the case of $BaTiO_3$, we have performed the present calculations using both forms (4) and (9) for the local field.

We have found it convenient to introduce reduced (dimensionless) variables

$$p = \mathcal{P}/N\mu$$

$$e = E/N\mu\lambda \tag{10}$$

$$t = T/T_o$$

(Note that the unit electric field $N\mu\lambda$ is the Lorentz local field (3) at zero applied field and saturation polarization). In terms of the reduced variables (10), Eqs. (1) and (2) take the form

$$p = \coth x - 1/x \ , \tag{11}$$

where

$$x = 3e_\ell/t = 3[e+f(p)]/t \tag{12}$$

The local field e_ℓ is obtained from either of Eqs. (4) or (9) so that

$$f(p) = \begin{cases} p + \frac{3}{5} t_1 p^3 + \frac{99}{175} t_2 p^5 + \ldots, \text{ power series} \\ \\ \dfrac{p}{1-\frac{3}{5} t_1 p^2} \ , \text{ Padé approximant} \ , \end{cases} \tag{13}$$

where we have used the obvious notation $t_i = T_i/T_o$. If the free energy is normalized as

$$g = \frac{G}{3NkT_o} \tag{14}$$

Eq. (5) becomes

$$g = \tfrac{1}{2}(t-1)\, p^2 + \tfrac{1}{4} b_o(t-t_1)\, p^4 + \tfrac{1}{6} c_o(t-t_2)\, p^6 + \ldots \ , \tag{15}$$

where $b_o = 3/5$, $c_o = 99/175$, etc. When g is defined as in (15), the

results analogous to Eqs. (7) and (8) are

$$c = \partial g/\partial p \tag{16}$$

and

$$1/\lambda\chi = \partial e/\partial p = \partial^2 g/\partial p^2 \tag{17}$$

The pyroelectric coefficient $\varphi = -(\partial P/\partial T)_E$ and the response figure of merit for a pyroelectric detector $M_1 = \varphi/\chi$ can also be expressed in terms of the reduced variables. This will be done in Section IV.

III STATIC PROPERTIES

A. Spontaneous Polarization.

In order to obtain the spontaneous polarization p_s (i.e. the polarization at zero applied field) as a function of temperature, it is necessary to solve the implicit relations (11)-(13) with e = 0. This must be done numerically, and two simple observations have proven most helpful here. First, for reasons which will become clear shortly, it is convenient to regard p rather t as the independent variable[5]. Second, Eq. (11) can then be solved numerically for x without regard to the form chosen for e_ℓ in Eqs. (12) and (13). The results for x as a function of p are shown in Fig. 1. In the numerical calculations, x was obtained by successive approximation, using Newton's method, until Eq. (11) was satisfied to an accuracy of one part in 10^9. Values of x, accurate to at least one part in 10^6, were obtained for $0 \leq p \leq 1$ at intervals of $\Delta p = 0.001$. These results can be used to obtain t from Eqs. (12) and (13), once a choice has been made for the form of e_ℓ and the values of the t_i. Figure 2 shows $p_s = P_s/N\mu$ as a function of temperature, using the power series form of e_ℓ for various values of t_1 with $t_i = 0$ for $i > 1$. As noted above, when $t_1 < 1$ the transition is second order, with p_s going continuously to zero as t increases toward 1. For $t_1 > 1$, however, there continue to exist nonzero solutions for p_s even for $t > 1$. There are, in fact, two such solutions, but it is easily shown that the smaller p_s, indicated by the broken curve in Fig. 2, corresponds to a negative susceptibility (see Section IV) and so is not stable. Although p_s is a double-valued function of t, the inverse relation, t as a function of p_s, is always single-valued, making the latter problem far easier to solve by numerical methods. As the temperature is increased, a point is

reached where the two solutions for p_s coincide, and above this temperature there are no solutions. This is the transition temperature (Curie temperature) t_c, and since the corresponding spontaneous polarization p_{sc} is nonzero, the transition produces a discontinuous change in p_s and so is first order.

Essentially similar results are obtained for the Padé approximant form of e_ℓ, as shown in Fig. 3. Since when p is small the Padé approximant reproduces the leading terms of the power series form of e_ℓ with the same value of t_1, the second-order transitions ($t_1 < 1$) exhibit essentially identical behavior in the two cases for $p \leq 0.2$. For larger polarizations, however, the increase in p_s with decreasing temperature for a given t_1 is always steeper in the Padé approximant case (the only exception occurs for $t_1 = 0$, when both forms of e_ℓ are identical to the Lorentz local field, and the conventional Weiss molecular field results are obtained). The two forms of e_ℓ can produce dramatically different results in first-order transitions ($t_1 > 1$), since only small increases in t_1 beyond 1 ($t_1 > 1.03$ in the Padé case, $t_1 > 1.08$ for the power series) are sufficient to make $p_{sc} > 0.2$.

The results shown in Figs. 2 and 3 are exact in the sense that they were obtained from numerical solutions of the exact equations (11)-(13). It is useful to compare them with results obtained using the approximations made in the phenomenological theory of ferroelectricity introduced by Devonshire[3] and widely used in fitting experimental data[6]. Devonshire assumed that the free energy can be expanded as a power series in the order parameter as suggested by Landau[7]. Since the polarization p is the order parameter, we may write

$$g = \tfrac{1}{2}\, ap^2 + \tfrac{1}{4}\, bp^4 + \tfrac{1}{6}\, cp^6 + \ldots , \qquad (18)$$

when the coefficients a,b,c,... are temperature dependent. In order to obtain a Curie-Weiss law for the susceptibility (17) above the Curie temperature, one must assume $a = a_o(t-1)$. Two further assumptions are now made in the Devonshire theory. The first is that the remaining coefficients b,c,... in Eq. (18) are temperature independent. This is not the case in the GMFT, but including the appropriate temperature dependence of these coefficients, as given by Eq. (15), introduces no major complications. The second assumption (which we refer to as the "Devonshire approximation") is that no serious error is made by neglecting terms in the power series (18) of order higher than p^6. It is the consequences of this second assumption which we wish to examine. When the series is truncated, Eq. (16) is used to obtain e, and e is then set equal to zero, we obtain for the spontaneous polarization

$$p_s^2 = -\frac{b}{2c}\left(1 \pm \sqrt{1 - 4\,\frac{ac}{b^2}}\right) \qquad (19)$$

For the GMFT, Eq. (19) becomes

$$p_s^2 = -\frac{35\delta_1}{66\delta_2}\left(1 \pm \sqrt{1 - \frac{44}{7}\,\frac{\delta_o \delta_2}{\delta_1^2}}\right) , \qquad (20)$$

where $\delta_i = t - t_i$ and $t_o = 1$. For $t_1 < 1$ only one choice of sign in (20) gives a real, positive value of p_s^2. For $t_1 > 1$ (first-order transitions) one obtains, as in the exact solution, only one real, positive value of p_s^2 for $0 \leq t \leq 1$, but two such values for $1 < t \leq t_c$. Again, the smaller p_s^2 leads to a negative susceptibility and is unphysical. Results for p_s as a function

of t with $t_2 = 0$ for several values of t_1 are shown in Fig. 4, where the solid curves were calculated using the Devonshire approximation and the exact results (broken curves) are given for comparison. One can readily see that, although the results of the Devonshire approximation approach the exact solution for small p_s, significant differences can appear for $p_s > 0.4$, and the discrepancy at a given value of t increases as t_1 increases. When t_1 is greater than one, so that the phase transition is first order, the polarization near the critical temperature quickly becomes so large that the results of the Devonshire approximation are no longer valid even close to the transition temperature (note the curves for $t_1=2$ in Fig. 4). Although the present results apply only to the GMFT, they strongly suggest that the Devonshire approximation should be used with caution when dealing with first-order phase transitions and that significant errors may occur in quantities calculated from an expansion of the free energy which has been truncated in the usual way.

B. Critical Temperature and Polarization.

Both $t_c = T_c/T_o$ and $p_{sc} = P_{sc}/N\mu$ can be obtained by locating the maximum in t as a function of p_s, and both increase with increasing t_1 as shown in Figs. 5 and 6. A more accurate method of determining t_c and p_{sc} has been found, however, and was used to calculate the values shown in the figures. This method is based on results for the pyroelectric coefficient and so will be discussed in Section IV.

An important point to be noted here is that the singularity in the Padé approximant form of e_ℓ for $t_1 \geq 5/3$ causes t_c to diverge and p_{sc} to approach 1 as t_1 increases toward 5/3 (indicated by the broken vertical line in Fig. 6). Hence, in this case, only values of $t_1 < 5/3$ can be

regarded as physically significant. It is interesting to note that when the power series form of e_ℓ is used p_{sc} never reaches 1, as it does for the Padé approximant form, but rather approaches a limit of approximately 0.746 as $t_1 \to \infty$.

IV. DYNAMIC PROPERTIES

A. Susceptibility.

The reduced inverse susceptibility $1/\lambda\chi$ defined in Eq. (17) can be obtained by differentiating Eq. (11) with respect to e and solving for $\partial e/\partial p$. The result is

$$1/\lambda\chi = \frac{t}{3p'} - f'(p) \ . \tag{21}$$

Here

$$p' = dp/dx = 1 - \coth^2 x + 1/x^2 \ , \tag{22}$$

where x is defined in Eq. (12), and

$$f'(p) = df/dp = \begin{cases} 1 + \frac{9}{5} t_1 p^2 + \frac{99}{25} t_2 p^4 + \ldots, \text{ power series} \\ \\ (1 + \frac{3}{5} t_1 p^2)/(1 - \frac{3}{5} t_1 p^2)^2, \text{ Padé approximant,} \end{cases} \tag{23}$$

where f(p) is defined in Eq. (13). Equations (21)-(23) have been used to calculate $1/\lambda\chi$ with e = 0 for various values of t_1, and the results are shown in Figs. 7 and 8, for the power series and Pade approximant forms of e_ℓ, respectively. (Note the logarithmic scale for $1/\lambda\chi$). In the Devonshire approximation we have

$$1/\lambda\chi = a + 3bp^2 + 5cp^4 \ , \tag{24}$$

and for the GMFT this becomes

$$1/\lambda\chi = \delta_o + \frac{9}{5} \delta_1 p^2 + \frac{99}{35} \delta_2 p^4 \ , \tag{25}$$

where $\delta_i = t - t_i$ as in Eq. (20). Using the Devonshire approximation (25),

we obtain the results shown in Fig. 9. As one might expect, all three calculations give similar results when the polarization is small, i.e. near the transition temperature for second-order transitions. As in the case of the spontaneous polarization, the differences increase with increasing polarization and are larger the greater the absolute value of t_1. It is interesting to note that the results for $t_1 = -1$ and $t_1 = 0$ clearly approach one another near the transition temperature in all three calculations, while the results for $t_1 = 1$ are distinctly different in the temperature range shown in Figs. 7-9. The reason for this will become clear as we examine in detail the behavior of $1/\lambda\chi$ in the vicinity of the transition temperature.

It is readily shown that the exact result, Eq. (21), leads to a Curie-Weiss law in the paraelectric phase. If all the quantities in (21) are expanded in power series in the polarization, we obtain

$$1/\lambda\chi = t - 1 + \frac{9}{5}(t-t_1)\, p^2 + \ldots \quad . \tag{26}$$

In the paraelectric phase the polarization p vanishes, and we obtain the Curie-Weiss law,

$$1/\lambda\chi = t - 1 \ . \tag{27}$$

If an electric field is applied to the paraelectric phase in order to induce a nonzero polarization, Eq. (24) shows that the change in $1/\lambda\chi$ will be proportional to p^2, in agreement with the Devonshire theory[5]. In addition, the GMFT predicts[1] that the coefficient of p^2 will be linear in t and vanish at the characteristic temperature t_1. This behavior has been observed experimentally by Drougard et al[8] and provides a means for determining t_1. Measurements are now in progress to confirm the results of Ref. 8 for $BaTiO_3$ ($t_1 \simeq 1.17$) and to obtain values of t_1 for other materials of interest.

In materials which undergo second-order transitions, p goes continuously to zero as $t \to 1$ from below, so that close to the transition temperature p can be arbitrarily small. Hence there exists a range of temperature in which it is possible to assume a more drastic form of the Devonshire approximation, namely that the term in the free energy (18) proportional to p^6 can be neglected as well as all the higher-order terms[3]. The spontaneous polarization is then given by $p_s^2 = - a/b$, which for the GMFT becomes

$$p_s^2 = - \frac{5(t-1)}{3(t-t_1)} \tag{28}$$

For e = o we can substitute (28) in (26) and obtain

$$1/\lambda\chi = - 2(t-1) , \tag{29}$$

which is the well-known result[3] that in second-order transitions the susceptibility has a Curie-Weiss behavior below as well as above the transition temperature, with the ratio of the slopes equal to -2. Figure 10 shows the results of the exact calculation using Eqs. (21)-(23) for several second-order transitions ($t_1 \leq 1$). Only the region near the transition temperature is shown, and the scale for $1/\lambda\chi$ is now linear. In this temperature range, the polarization is small enough that the power series and Padé approximant forms of e_i, as well as the Devonshire approximation, yield essentially identical results except for the case of $t_1 = 1$ which will be discussed below. Since the result (27) is exact for the paraelectric phase, the behavior of $1/\lambda\chi$ is the same for both forms of e_i and all values of t_1. In the ferroelectric phase, Eq. (29) is correct through terms of order p^2, so that its validity can extend over

a substantial temperature range, especially for small values of t_1 which, as noted above, lead to a relatively gradual increase in polarization as the temperature is lowered.

The case $t_1 = 1$ must be treated separately because its critical behavior is different from that of other second-order transitions. Equation (26), which predicts that the spontaneous polarization has the temperature dependence $p_s^2 \propto 1-t$, fails in this case. Using Eq. (20) with $\delta_o = \delta_1 = t-1$, one can show that the critical behavior is actually $p_s^4 \propto 1-t$. One effect of this change in critical exponent is readily seen in Figs. 2-4, where the curvature of t as a function of p_s vanishes at $t_1 = 1$. The unique critical behavior of $1/\lambda\chi$ for $t_1=1$ is clearly visible in Fig. 10, where the Padé approximant form of e_ℓ (solid curve), power series form of e_ℓ (broken curve), and Devonshire approximation (dash-dot curve), yield significantly different results. Unusual critical behavior for the case $t_1=1$ should not be surprising, since the point $(p,t,t_1) = (0,1,1)$ is a tricritical point in the sense of Griffiths[9], and the critical exponents at such a point may differ from those at neighboring points. A detailed study of the critical behavior for $t_1=1$ is now in progress.

A final word should be said about the low-temperature behavior of $1/\lambda\chi$. In the exact results (Fig. 7 and 8), $1/\lambda\chi$ diverges as $t \to 0$, reflecting the fact that $\chi \to 0$ as the polarization saturates. For the Devonshire approximation, the results are rather peculiar and unphysical. It can be shown with the aid of Eq. (20) that for $t_1 < 0$ and $t_2 = 0$, we have $p_s^2 \to -5/3t_1$ as $t \to 0$. Thus p_s saturates, but at a value which depends on t_1 rather than at $p_s = 1$. If this finite limit for p_s is substituted in Eq. (24), one obtains a finite limit for $1/\lambda\chi$ rather than a divergence (see the curve for $t_1 = -1$ in Fig. 9). On the other hand, if $t_1 > 0$,

both the polarization (20) and the inverse susceptibility (24) diverge as $t \to 0$. We conclude, therefore, that the Devonshire approximation must always fail at low temperatures: either the polarization or the susceptibility will behave in an unphysical manner.

B. Pyroelectric Coefficient.

In terms of the reduced variables (10), one can define a reduced pyroelectric coefficient

$$\varphi^* = - (\partial p/\partial t)_e \ , \tag{30}$$

which is related to the conventional pyroelectric coefficient $\varphi = - (\partial P/\partial T)_E$ by

$$\varphi^* = \frac{T_o}{N\mu} \varphi \ . \tag{31}$$

In the following we discuss φ^* only for $e = 0$, which corresponds to the usual experimental situation. It should be noted, however, that an applied electric field produces significant changes in φ^* and can induce a pyroelectric effect above the Curie temperature[10]. These effects will be discussed in a future report.

An exact expression for φ^* can be obtained by differentiating Eq.(11) with respect to t and solving for $\partial p/\partial t$. The result is

$$\varphi^* = \frac{xp'}{t-3p'f'(p)} \tag{32}$$

where p' and f' are defined in Eqs. (22) and (23). The pyroelectric coefficient calculated from (32) with $e = 0$ ($p=p_s$) is shown as a function of

reduced temperature in Figs. 11 and 12 for various values of the characteristic temperature t_1, using the power series and Padé approximant forms of the local field, respectively.

In the Devonshire approximation, the reduced pyroelectric coefficient for $e = 0$ is[1]

$$\varphi^* = \frac{a'+b'p_s^2+c'p_s^4}{2p_s(b+2cp_s^2)} \quad , \tag{33}$$

where the prime indicates differentiation with respect to t. For the GMFT this becomes

$$\varphi^* = \frac{1 + \frac{3}{5} p_s^2 + \frac{99}{175} p_s^4}{2p_s(\frac{3}{5} \delta_1 + \frac{198}{175} \delta_2 p_s^2)} \quad , \tag{34}$$

where $\delta_i = t-t_i$ as in Eq. (20). The results of Eq. (34) are shown in Fig. 13 for the same values of t_1 used in the calculations of Fig. 11 for the power series form of e_ℓ.

The exact results shown in Figs. 11 and 12 are fully consistent with the polarization curves in Figs. 2 and 3. Large values of t_1 produce a flat polarization curve (and hence small φ^*) at low temperatures, followed by a sharp drop in p_s giving a large φ^* near the transition temperature. For small t_1, φ^* is relatively larger at low temperature and smaller near the transition, giving rise to the crossings of the φ^* curves for $t_1 < 1$ which characterize the results in Figs. 11 and 12. Note also that the steeper polarization curves produced by the Padé approximant form of e_ℓ lead to smaller values of φ^* at low temperatures and larger values near the transition than are obtained with the power series form.

Here again the Devonshire approximation fails to give results consistent with the exact solutions (see Fig. 13). For $t_1 \geq 0$, the pyroelectric coefficient diverges as $t \to 0$. This is due to the unphysical divergence of p_s noted above in connection with the susceptibility. Unfortunately, this low-temperature divergence is stronger than the one at the transition temperature and dominates the behavior of φ^* throughout most of the temperature range. The crossings obtained in the exact results are eliminated, and the range in which the approximation yields satisfactory results is even smaller than in the case of the polarization or susceptibility.

Equation (32) for the pyroelectric coefficient provides the basis for an accurate calculation of the temperature t_c at which a first-order transition occurs when $t_1 > 1$. As can be seen in Figs. 2-4, t_c corresponds to the "nose" of the polarization curve, beyond which no nonzero solutions of Eqs. (11)-(13) exist. At this point $\partial p_s/\partial t$ diverges. This cannot happen for $p_s < 1$ unless the denominator of Eq. (32) vanishes. Thus the transition temperature t_c and the spontaneous polarization at that temperature p_{sc} are related by

$$t_c = 3\, p'_{sc}\ \ f'(p_{sc}) \ , \tag{35}$$

where p'_{sc} is simply p' as defined in Eq. (22) evaluated at $e = 0$ and $t = t_c$, and f' is defined in Eq. (23). Now Eq.(12) gives a second relation between t_c and p_{sc}:

$$t_c = 3\ \ f(p_{sc})/x_{sc} \ , \tag{36}$$

where, as usual, the subscripts s and c indicate $e = 0$ and $t = t_c$, respectively. We have found it most convenient to eliminate t_c from Eqs. (35) and

(36) and to solve for t_1 as a function of p_{sc} (assuming, in the power series form of e_ℓ, that $t_i = 0$ for $i > 1$). This gives

$$t_1 = \frac{5}{3} \frac{p_{sc} - x_{sc}\, p'_{sc}}{D\, p_{sc}^2} , \tag{37}$$

where

$$D = \begin{cases} 3\, x_{sc}\, p'_{sc} - p_{sc} , & \text{power series} \\ \\ x_{sc}\, p'_{sc} + p_{sc} , & \text{Padé approximant} . \end{cases} \tag{38}$$

By regarding p_{sc} as the independent variable, solving (37) and (38) for t_1 and then evaluating t_c from (36), one obtains the results shown in Figs. 5 and 6.

C. Response Figure of Merit

It is well-known that the sensitivity of a pyroelectric detector is proportional to the ratio $M_1 = \varphi/\chi$, often referred to as the response figure of merit. In terms of reduced variables, the corresponding ratio is

$$m_1 = \varphi^*/\lambda\chi , \tag{39}$$

which is related to the conventional figure of merit by

$$m_1 = \frac{T_o}{N_\mu \lambda} M_1 . \tag{40}$$

Combining Eqs. (21) and (32) gives the simple result,

$$m_1 = x/3. \tag{41}$$

In the following we will discuss the figure of merit at zero applied electric field. This is the simplest case and corresponds to the situation encountered in most detector applications, but it should be noted that pyroelectric

detectors have been constructed which require a d.c. bias field, and the characteristics of this mode of operation have been analyzed.[11]

Using Eq. (41), we have calculated m_1 as a function of temperature for various values of t_1, using the power series form of e_ℓ (with $t_i = 0$ for $i > 1$) and using the Padé approximant form. The results, shown in Figs. 14 and 15, are quite similar for the two forms of the local field. The divergence of m_1 as $t \to 0$ is due to the fact that φ^* remains finite while χ goes to zero. This results from the assumption, implicit in Eq. (1), that the elementary dipoles can assume any orientation in space, that is they behave "classically" as in the "infinite-spin" limit of the Weiss theory of ferromagnetism. Other, equally plausible, assumptions lead to the result that $\varphi^* \to 0$ as $t \to 0$. We will return to this point shortly. From a practical point of view, this enhancement of m_1 may not be useful, even if correct, simply because the <u>total</u> susceptibility can never vanish, but will instead be dominated, as p_s saturates, by the electronic and non-ferroelectric lattice contributions which are neglected in the present model.

In the Devonshire approximation, Eq. (39) becomes[1]

$$m_1 = a' p_s + b' p_s^3 + c' p_s^5 , \tag{42}$$

where the prime again indicates differentiation with respect to t. For the GMFT, Eq. (42) yields

$$m_1 = p_s \left(1 + \frac{3}{5} p_s^2 + \frac{99}{175} p_s^4\right) , \tag{43}$$

from which we have calculated the results shown in Fig. 16. For small values of t_1 the Devonshire approximation is in reasonable agreement with the exact results at sufficiently high temperatures, indicating considerable cancellation of the errors occurring in φ^* and $1/\lambda\chi$ separately. This might

be expected from the fact that Eq. (43) is correct up to terms of order p_s^5.

There remains one extremely important point to be made concerning Eq. (41). Since m_1 depends only on x, which in turn depends only on p_s via Eq. (11), we conclude that m_1 depends only on p_s. In this case, regarding the polarization as the independent variable is more than the computational convenience it has been up to this point. Regarding m_1 as a function of p_s predicts a universal behavior of the figure of merit as a function of the spontaneous polarization, independent of the choice of a form for the local field (and so necessarily independent of the values of the t_i). This is shown in Fig. 17, where m_1 is given as a function of $1-p_s$ for the "classical" case described by $p = \coth x - 1/x$ (see curve labelled $J = \infty$). The variable $1-p_s$, which increases with temperature, is used rather than p_s so that comparison can be made with Figs. 14-16. In addition, we have calculated m_1 for the "spin-$\frac{1}{2}$" case in which the polarization is given by $p = \tanh x$, and for the Devonshire approximation to the "classical" case. These are indicated in Fig. 17 by the curve labelled $J = \frac{1}{2}$ and the broken curve, respectively. (Note that for $J = \frac{1}{2}$ we find that m_1 remains finite as $t \to 0$. This is because $\varphi^* \to 0$ as $t \to 0$ in this case.) Perhaps surprisingly, the three results are indistinguishable for $p_s \leq 0.5$. So while Eq. (41) provides a direct test of whether the dipoles behave classically or have only certain allowed orientations, this information can be obtained only from measurements made near saturation polarization, that is in the low-temperature region which has not previously been of sufficient interest to warrant detailed experimental study. Low-temperature measurements of the pyroelectric coefficient and susceptibility (corrected for electronic and non-ferroelectric lattice contributions) are planned for the near future.

Equations (40) and (41) predict that for a given polarization the experimental response figure of merit M_1 should scale from one material to another as $N\mu\lambda/T_o$. Data is now being collected to check this prediction which, if verified, could serve as a useful guide in obtaining larger values of M_1.

Finally, it is interesting to note that the scale factor in Eq. (40) can be written, with the aid of Eq. (6), as

$$\frac{T_o}{N\mu\lambda} = \frac{\mu}{3k} . \tag{44}$$

Thus the experimental figure of merit M_1 is inversely proportional to the dipole moment μ. Since the left-hand side of Eq. (44) can be calculated from experimental quantities (saturation polarization, Curie coefficient, and Curie-Weiss temperature), we can now determine μ indirectly. The value of Eq. (44) may be greatly increased if it proves possible to calculate μ directly from lattice dynamical models.

V. COMPARISON WITH EXPERIMENT

A detailed comparison of the predictions of the GMFT presented above with the experimental data available in the literature is now in progress and will be the subject of a future report. The preliminary phase of this comparison has already yielded some important information and conclusions which will be described here.

As noted in Section IVA, the characteristic temperature t_1 can be determined from the electric field dependence of $1/\lambda\chi$. This has been done to date for only one material, however, so that it would be most valuable to have another method of finding t_1 from data already available in the literature. In the case of a first-order phase transition, the transition temperature t_c depends on t_1 as shown in Figs. 5 and 6 for the power series and Padé approximant forms of the local field, respectively. Hence, in this case t_1 can be determined from the observed value of t_c. Unfortunately, many materials of interest, such as triglycine sulfate (TGS) and its isomorphs, undergo second-order transitions which occur at $t = 1$ independent of the value of t_1. So yet another method of finding t_1 is needed, and our preliminary results indicate that fitting the temperature dependence of the spontaneous polarization p_s can be used for this purpose.

Figure 18 shows the experimental results of Triebwasser[12] for the spontaneous polarization of TGS as a function of temperature (both in reduced units). The solid curve is the prediction of the GMFT, using the Padé approximant form of the local field with $t_1 = 0.85$. The agreement between theory and experiment is well within the experimental error. The value $t_1 = 0.85$ was determined by trial and error, using variations of $\Delta t_1 = 0.05$. The fit for $t_1 = 0.85$ is significantly better than for $t_1 = 0.80$ or $t_1 = 0.90$, but the amount of computation required for further

refinement is too great to be performed by hand. A computer program is now being written to carry out a least-squares fit and determine t_1 to the greatest precision compatible with the accuracy of the experimental data.

Our preliminary result, $t_1 = 0.85 \pm 0.03$ for TGS, can also be obtained from considerations based on the Devonshire approximation. The more drastic form of this approximation, neglecting terms in the free energy (18) of order p^6 and higher, leads (for the GMFT) to Eq. (28) which can be solved for t_1 as a function of p_s and t:

$$t_1 = t + \frac{5}{3p_s^2} \quad (t-1) \tag{45}$$

Averaging the three experimental points in Fig. 18 having the smallest values of p_s yields $t_1 = 0.84$, in good agreement with the trial-and-error fit shown in Fig. 18.

Even though the computer program required to obtain optimum values of t_1 from the observed temperature dependence of p_s is not yet completed, it is already possible to draw certain conclusions from the preliminary fit for TGS. First, the Padé approximant form of the local field e_ℓ gives a significantly better fit than does the power series form. The value $t_1 \simeq 0.84$ obtained for small p_s from the Devonshire approximation is independent of the form chosen for e_ℓ, but when this value is used to calculate p_s for small t (i.e. large p_s), the Padé approximant form of e_ℓ gives results in good agreement with experiment (see Fig. 18) while the power series form with $t_i = 0$ for $i > 1$ results in large deviations from experiment when p_s is greater than approximately 0.5.

Second, the relatively large value of t_1 obtained for TGS confirms the superiority of the GMFT to the conventional molecular field theory

(which is identical to the GMFT with $t_1 = 0$ for all i). In the context of the GMFT, the phase transition in TGS is "nearly first order" since $t_1 > 1$ results in first-order transitions. The onset of the spontaneous polarization for $t \lesssim 1$ is far steeper than predicted by the conventional molecular field theory and cannot be accounted for without introducing the generalized molecular field described by Eq. (4).

Finally, the success of the GMFT in fitting the spontaneous polarization of TGS encourages us to believe that the susceptibility, pyroelectric coefficient, and figure of merit of this material, as well as the properties of other ferroelectrics, can be predicted from the GMFT. An extensive program, mentioned above, is now in progress to compare the predictions of the GMFT with published experimental results and with those obtained in our laboratory.

VI. SUMMARY

The investigations described in this report were undertaken with the goal of elucidating the physical mechanism responsible for the pyroelectric effect in ferroelectric crystals, in the hope that an understanding of this mechanism would lead to practical guidelines for the selection of infrared detector materials and to greater insight into the factors which limit the performance of pyroelectric detectors. We have reported previously[1,2] on an important generalization of the well-known molecular field theory of ferroelectricity. (These results are summarized briefly in Section II.) With this generalization it is possible to overcome the major objections which have been raised to the use of a molecular field theory in this context[1]. Much of the work reported here is of an essentially technical nature: the generalized molecular field theory (GMFT) is used to obtain exact expressions for the ferroelectric properties of crystals (spontaneous polarization, dielectric susceptibility, critical temperature and polarization) and for the resulting pyroelectric properties (pyroelectric coefficient and response figure of merit for radiation detection). These results are presented in Sections III and IV for various values of the parameters which appear in the GMFT. An extensive comparison of these predictions with the available experimental data is now under way, and some highly encouraging results obtained in the preliminary stages of this work are reported in Section V.

Two major qualitative results have emerged, however, from these quantitative considerations. In Section II we introduce a set of reduced (dimensionless) variables which greatly simplify the calculations, and in Section III we find that regarding the polarization rather than the temperature as the independent variable results in a large saving of computational effort. When we turn our attention to the response figure of merit for

pyroelectric detectors (Section IV), we find that these two devices are not merely convenient computational aids. Rather, they lead directly to a striking universal behavior for the figure of merit. We find that the figure of merit, in reduced units, is always given by the same universal function of the polarization, independent of the many details of the GMFT which can vary from one material to another and affect the behavior of other properties such as the susceptibility or pyroelectric coefficient. Work is now in progress to verify experimentally this universal behavior and to determine whether it can be exploited as a tool for optimizing the response figure of merit.

Also, we have compared the exact results of the GMFT with the Devonshire formalism obtained from the GMFT by truncating the power-series expansion for the free energy. Our results show that in general the Devonshire formalism is a poor approximation to the GMFT, especially for first-order transitions. Only in the case of the response figure of merit are the results of this approximation accurate over a wide enough range of polarization to be considered useful.

References

1. M.I. Bell and P.M. Raccah, Technical Report ECOM-74-0470-1, Yeshiva University (1975).
2. M.I. Bell and P.M. Raccah, Bull. Am. Phys. Soc. 20, 349 (1975).
3. A.F. Devonshire, Advan. Phys. 3, 85 (1954).
4. L. Onsager, J. Am. Chem. Soc. 58, 1486 (1936).
5. G.J. Iafrate, private communication. See also, G.J. Iafrate, F. Rothwarf, and M.I. Bell, Bull. Am. Phys. Soc. 20, 503 (1975).
6. See, for example, E. Fatuzzo and W.J. Merz, in Selected Topics in Solid State Physics, ed. by E.P. Wolforth (J. Wiley and Sons, New York, 1967), vol. 7, chap. 3.
7. L.D. Landau and E.M. Lifshitz, Statistical Physics (Pergamon Press, London, 1958) chap. 14.
8. M.E. Drougard, R. Landauer, and D.R. Young, Phys. Rev. 98, 1010 (1955).
9. R.B. Griffiths, Phys. Rev. Letters 24, 715 (1970).
10. A.G. Chynoweth, J. Appl. Phys. 27, 78 (1956).
11. A. van der Ziel, Final Report on ARPA Contract DAAK 02-72-C-0398, University of Minnesota, April 1974.
12. S. Triebwasser, I.B.M. J. Res. Dev. 2, 212 (1958).

Figure Captions

Fig.1 - Solutions of the polarization equation $p = \coth x - 1/x$.

Fig.2 - The spontaneous polarization $p_s = P_s/N\mu$ as a function of the reduced temperature $t = T/T_o$ for the power series form of the local field e_ℓ and various values of the characteristic temperature $t_1 = T_1/T_o$ (with $t_i = 0$ for $i > 1$).

Fig.3 - The spontaneous polarization $p_s = P_s/N\mu$ as a function of the reduced temperature $t = T/T_o$ for the Padé approximant form of the local field e_ℓ and various values of the characteristic temperature $t_1 = T_1/T_o$.

Fig.4 - The spontaneous polarization $p_s = P_s/N\mu$ as a function of the reduced temperature $t = T/T_o$ calculated in the Devonshire approximation (solid curves) is compared with the exact results using the power series form of the local field e_ℓ. The same values of the characteristic temperature $t_1 = T_1/T_o$ are used as in Fig. 2, with $t_i = 0$ for $i > 1$.

Fig.5 - The Curie temperature $t_c = T_c/T_o$ and the spontaneous polarization at the Curie temperature $p_{sc} = P_{sc}/N\mu$ as a function of the characteristic temperature $t_1 = T_1/T_o$ (with $t_i = 0$ for $i > 1$) using the power series form of the local field e_ℓ.

Fig.6 - The Curie temperature $t_c = T_c/T_o$ and the spontaneous polarization at the Curie temperature $p_{sc} = P_{sc}/N\mu$ as a function of the characteristic temperature $t_1 = T_1/T_o$ using the Padé approximant form of the local field e_ℓ.

Fig.7 - The reduced inverse susceptibility $1/\lambda\chi = \partial e/\partial p$ at $e = 0$ (note logarithmic scale) as a function of the reduced temperature $t = T/T_o$ for the power series form of the local field e_ℓ and various values of the characteristic temperature $t_1 = T_1/T_o$ (with $t_i = 0$ for $i > 1$).

Fig.8 - The reduced inverse susceptibility $1/\lambda\chi = \partial e/\partial p$ at $e = 0$ (note logarithmic scale) as a function of the reduced temperature $t = T/T_o$ for the Padé approximant form of the local field e_ℓ and various values of the characteristic temperature $t_1 = T_1/T_o$.

Fig.9 - The reduced inverse susceptibility $1/\lambda\chi = \partial e/\partial p$ at $e = 0$ (note logarithmic scale) as a function of the reduced temperature $t = T/T_o$, calculated in the Devonshire approximation. The same values of the characteristic temperature $t_1 = T_1/T_o$ are used as in Fig. 7, with $t_i = 0$ for $i > 1$.

Fig.10- The reduced inverse susceptibility $1/\lambda\chi = \partial e/\partial p$ at $e = 0$ (note linear scale) as a function of the reduced temperature $t = T/T_o$ in the region near the transition temperature, for selected second-order transitions ($t_1 = T_1/T_o \leq 1$). For $t > 1$ and for $t < 1$ with $t_1 < 1$, the power series and Padé approximant forms of the local field e_ℓ give essentially identical results. For $t_1 = 1$ the results of the Padé approximant, power series, and Devonshire approximation are indicated by the solid, broken, and dash-dot curves, respectively.

Fig.11- The reduced pyroelectric coefficient $\varphi^* = -(\partial p_s/\partial t)$ as a function of the reduced temperature $t = T/T_o$ for the power series form of the local field e_ℓ and various values of the characteristic temperature $t_1 = T_1/T_o$ (with $t_i = 0$ for $i > 1$).

Fig.12- The reduced pyroelectric coefficient $\varphi^* = -(\partial p_s/\partial t)$ as a function of the reduced temperature $t = T/T_o$ for the Padé approximant form of the local field e_ℓ and various values of the characteristic temperature $t_1 = T_1/T_o$.

Fig.13- The reduced pyroelectric coefficient $\varphi^* = -(\partial p_s/\partial t)$ as a function of the reduced temperature $t = T/T_o$, calculated on the Devonshire

approximation. The same values of the characteristic temperature $t_1 = T_1/T_o$ are used as in Fig. 11, with $t_i = 0$ for $i > 1$.

Fig.14 - The reduced response figure of merit $m_1 = \varphi^*/\lambda\chi$ at zero applied field as a function of the reduced temperature $t = T/T_o$ for the power series form of the local field e_ℓ and various values of the characteristic temperature $t_1 = T_1/T_o$ (with $t_i = 0$ for $i > 1$).

Fig.15 - The reduced response figure of merit $m_1 = \varphi^*/\lambda\chi$ at zero applied field as a function of the reduced temperature $t = T/T_o$ for the Padé approximant form of the local field e_ℓ and various values of the characteristic temperature $t_1 = T_1/T_o$.

Fig.16 - The reduced response figure of merit $m_1 = \varphi^*/\lambda\chi$ at zero applied field as a function of the reduced temperature $t = T/T_o$, calculated in the Devonshire approximation. The same values of the characteristic temperature $t_1 = T_1/T_o$ are used as in Fig. 14, with $t_i = 0$ for $i > 1$.

Fig.17 - The reduced response figure of merit $m_1 = \varphi^*/\lambda\chi$ at zero applied field as a function of $1 - p_s$, showing its universal behavior. The curves $J = \frac{1}{2}$ and $J = \infty$ correspond to the polarization equations $p = \tanh x$ and $p = \coth x - 1/x$, respectively. The broken curve represents the Devonshire approximation to the $J = \infty$ case.

Fig.18 - Comparison of the spontaneous polarization of triglycine sulfate as measured by Triebwasser (Ref. 12) with the prediction of the GMFT using the Padé approximant form of the local field and $t_1 = 0.85$

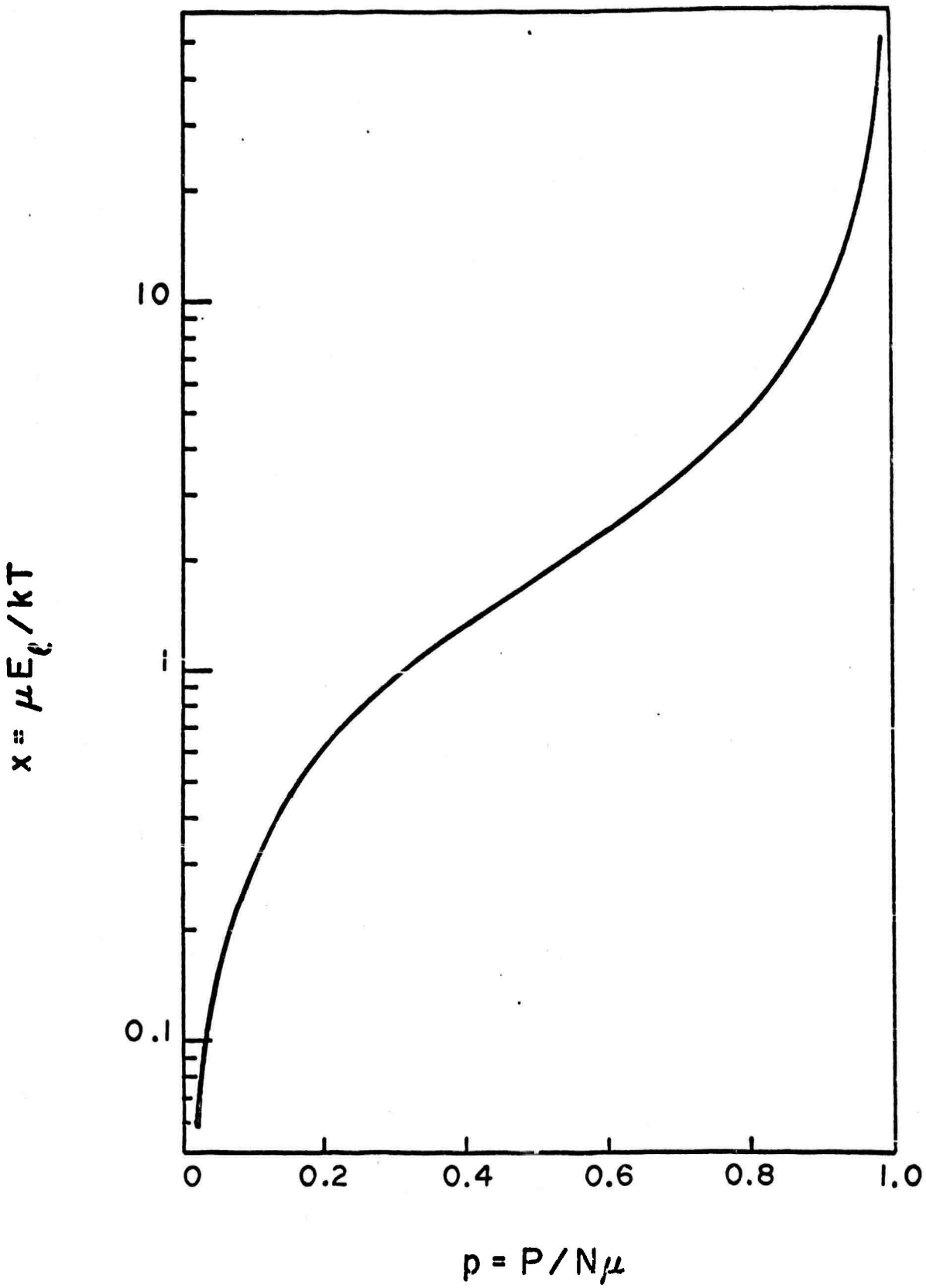

Fig. 1

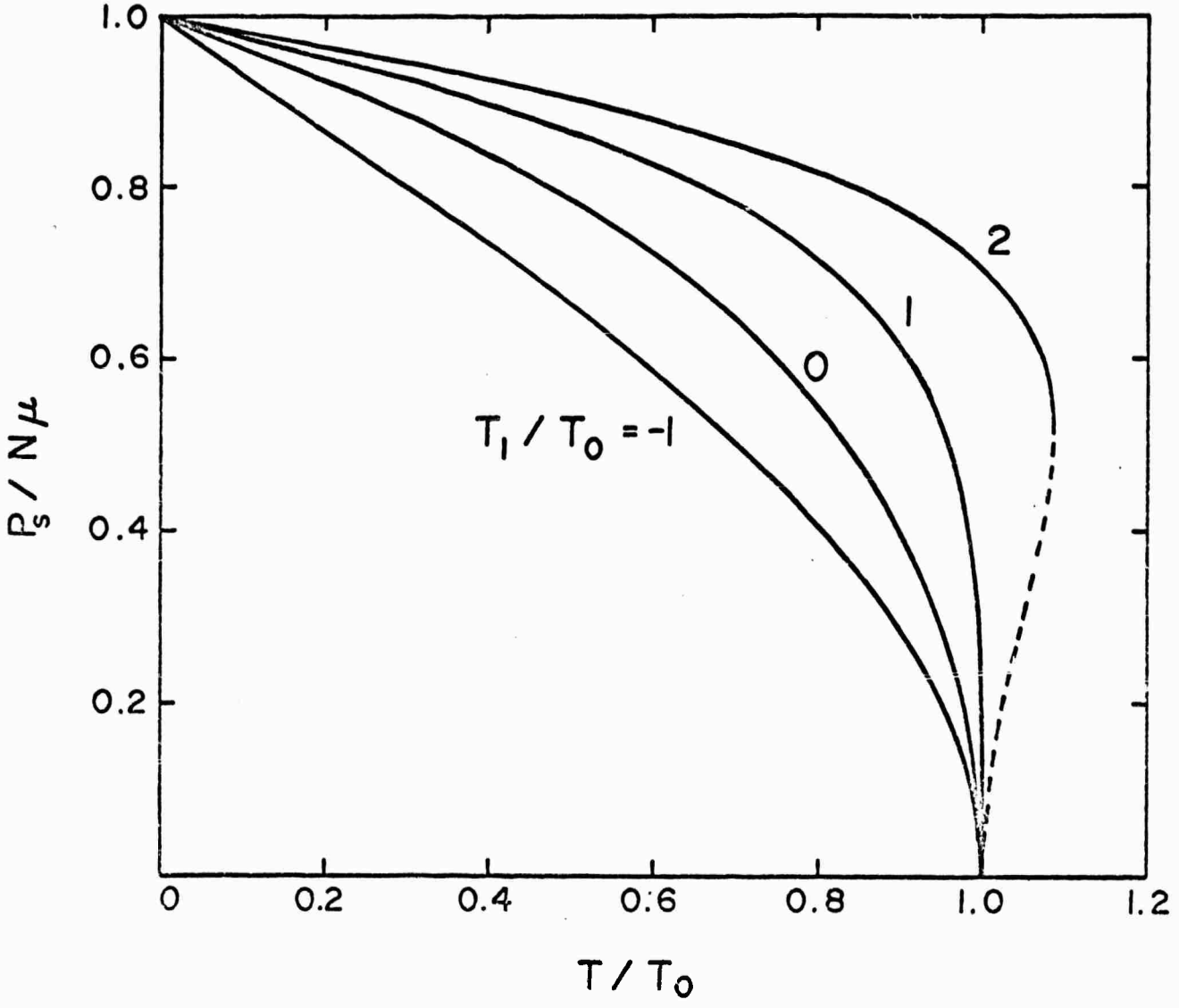

Fig. 2

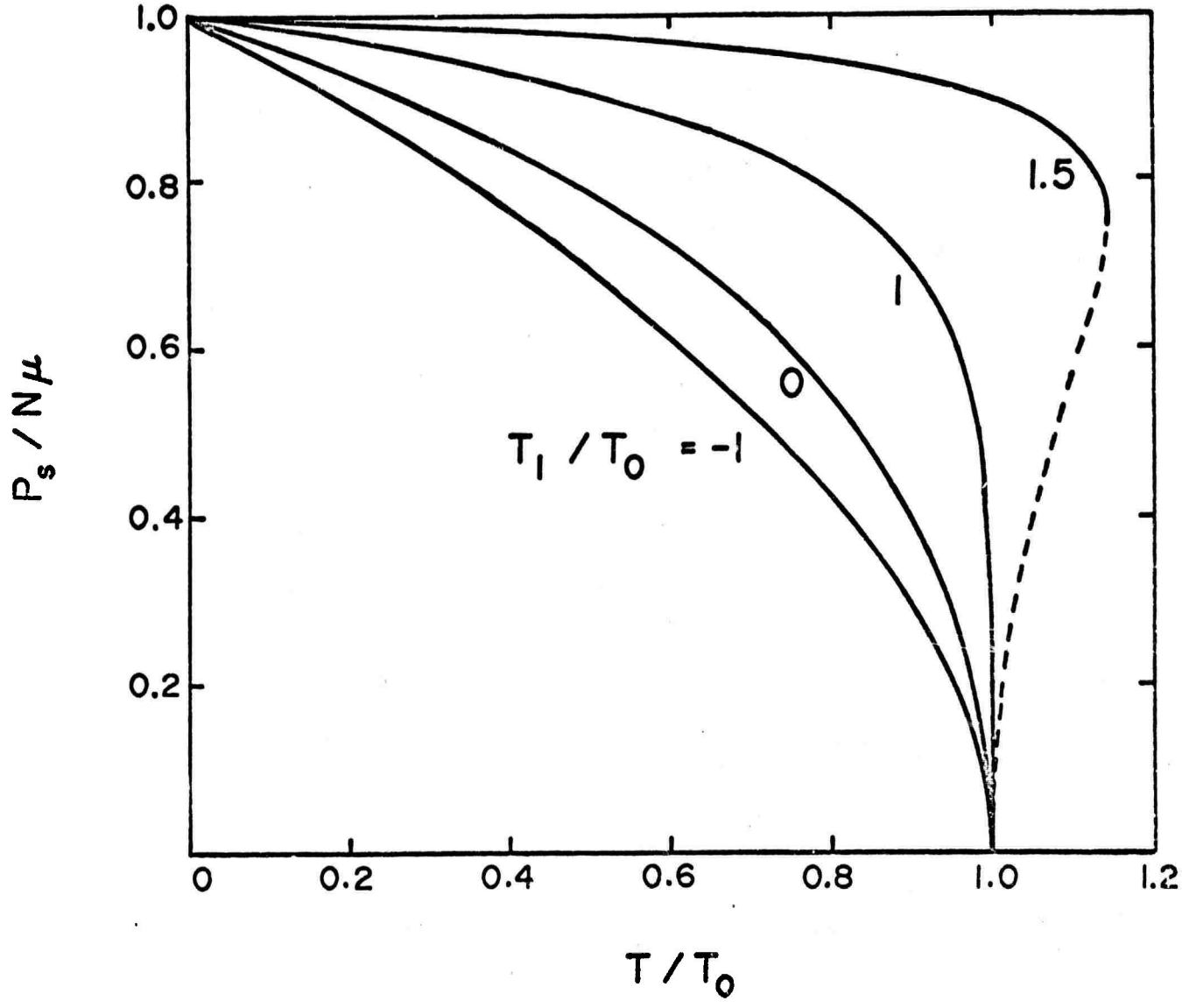

Fig. 3

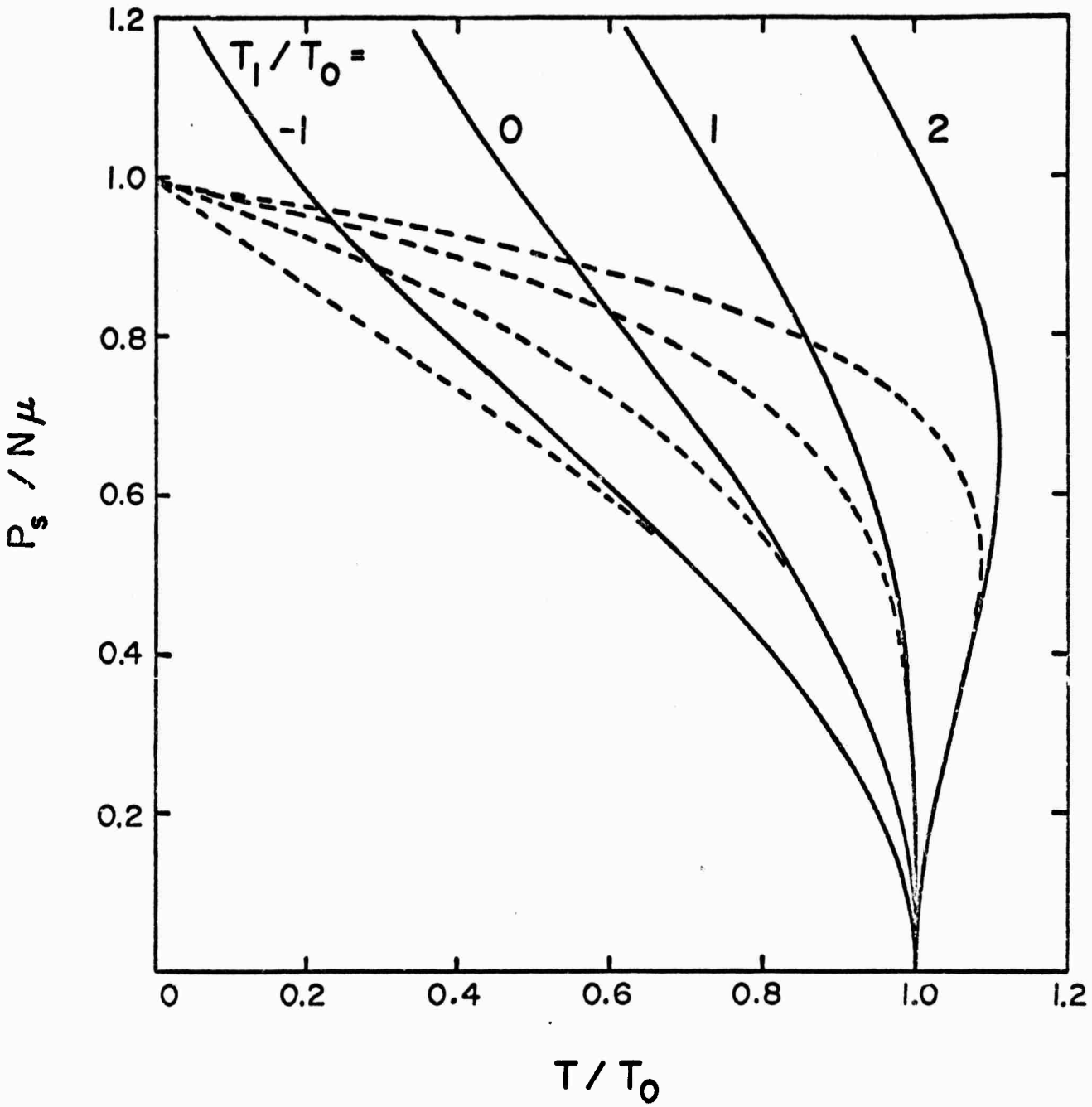

Fig. 4

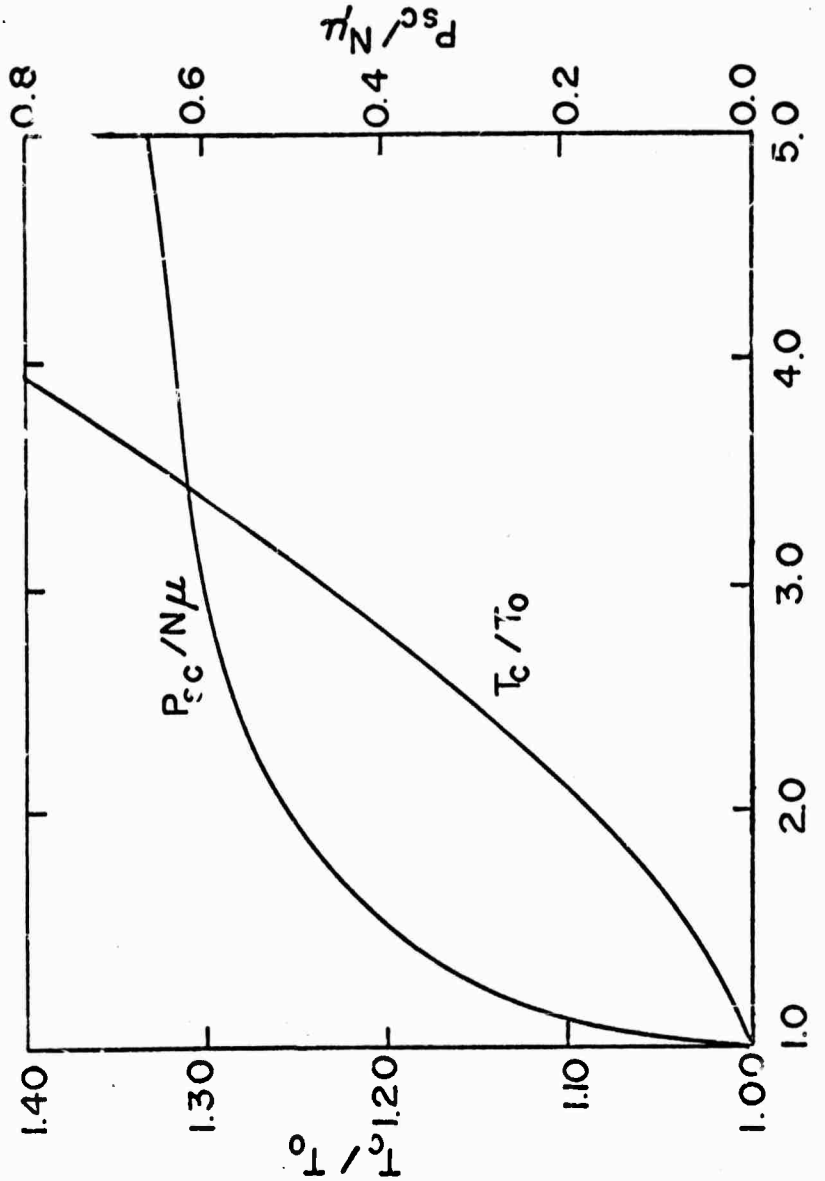
$P_{sc}/N\mu$
T_c/T_o
T_c/T_o
$P_{sc}/N\mu$
T_1/T_0
1.00
1.10
1.20
1.30
1.40
1.0
2.0
3.0
4.0
5.0
0.0
0.2
0.4
0.6
0.8

Fig. 5

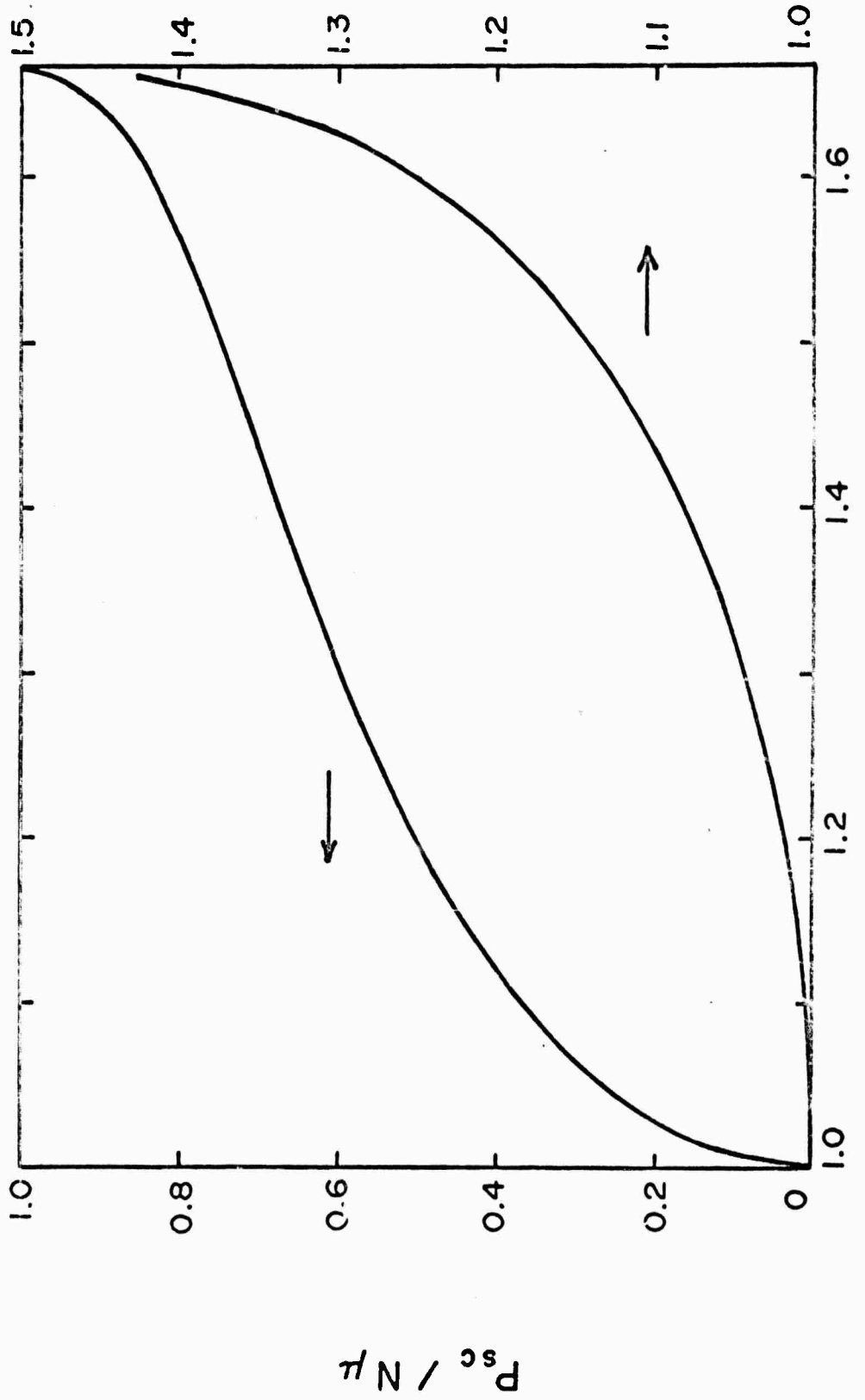

Fig. 6

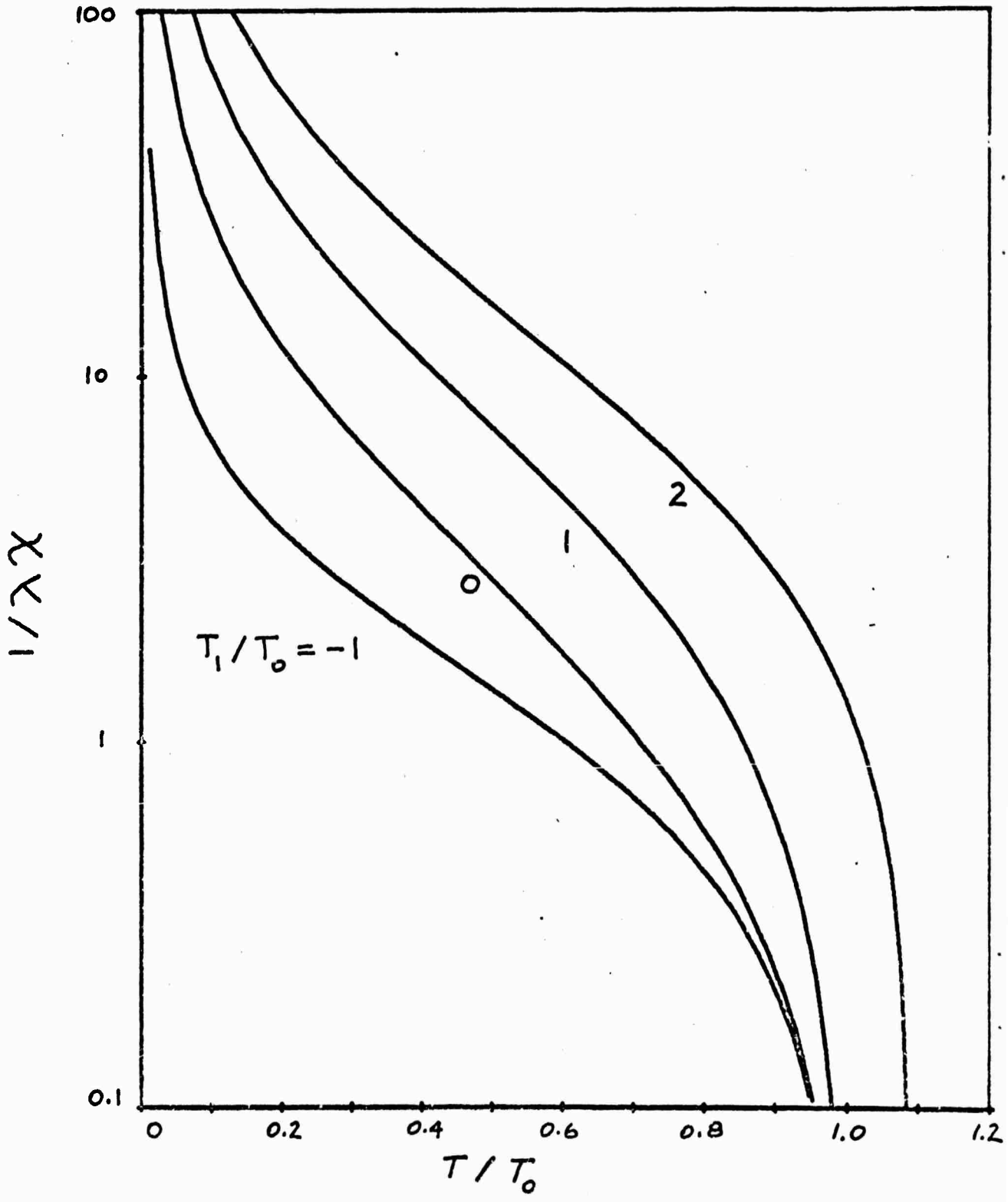

Fig. 7

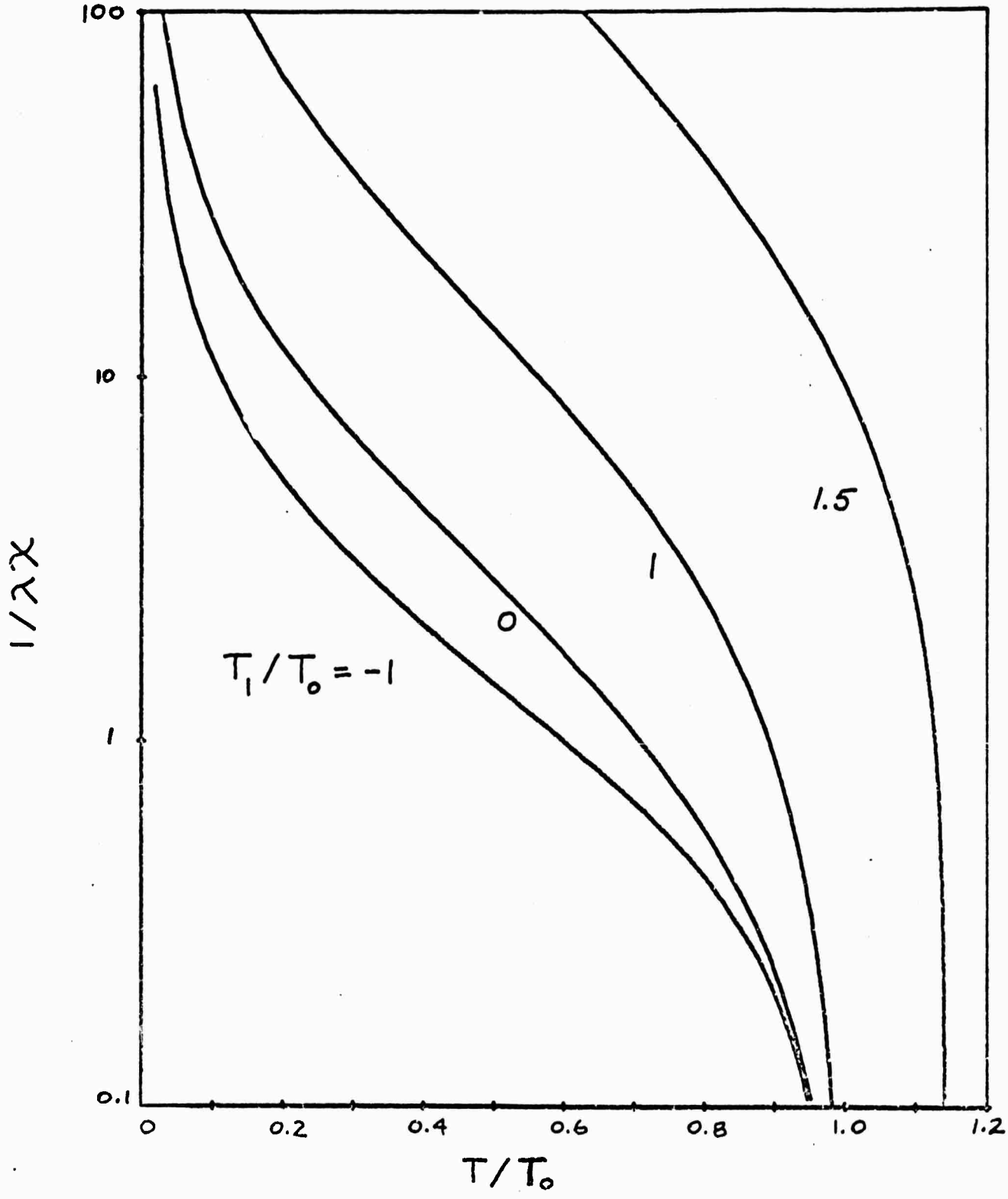

Fig. 8

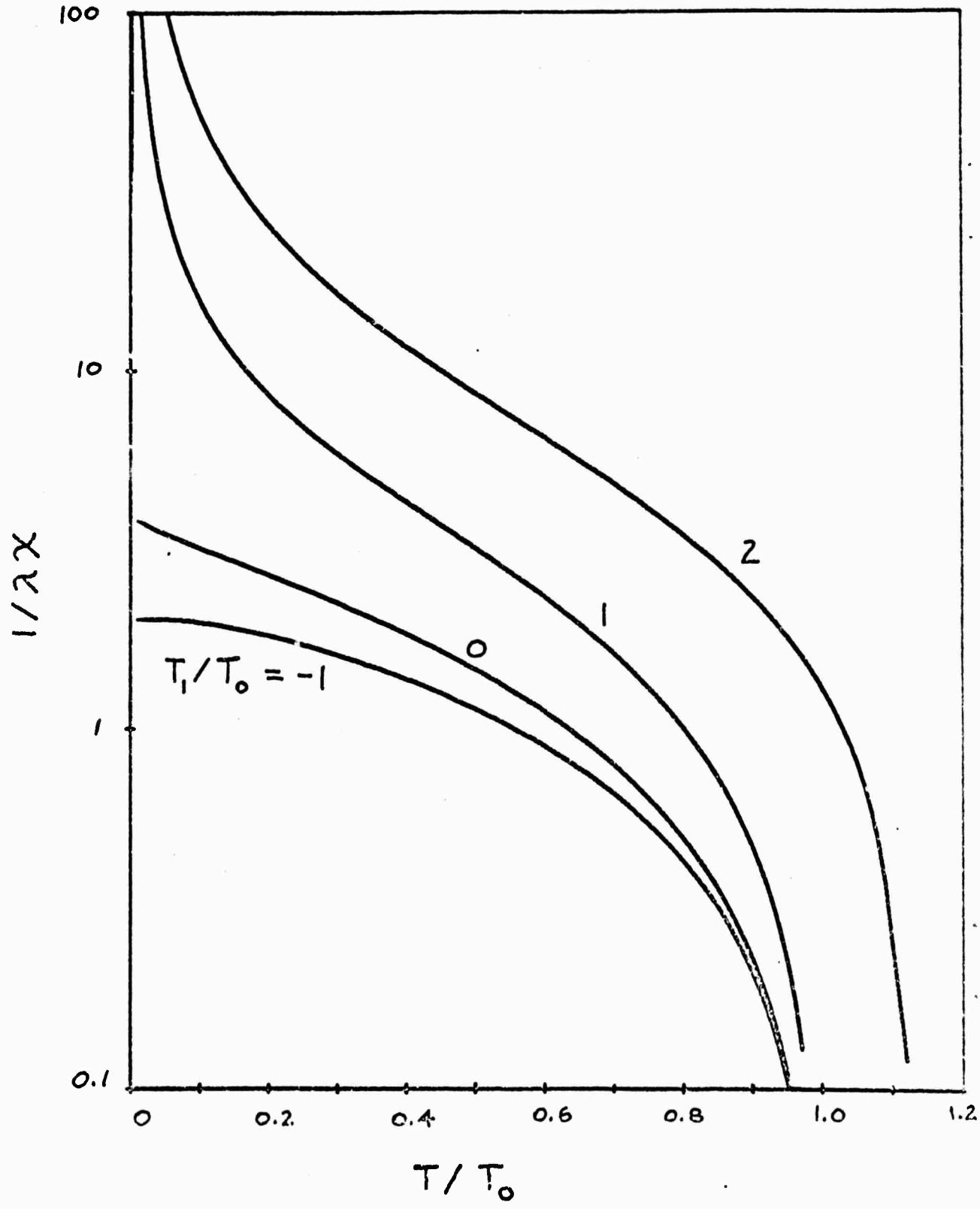

Fig. 9

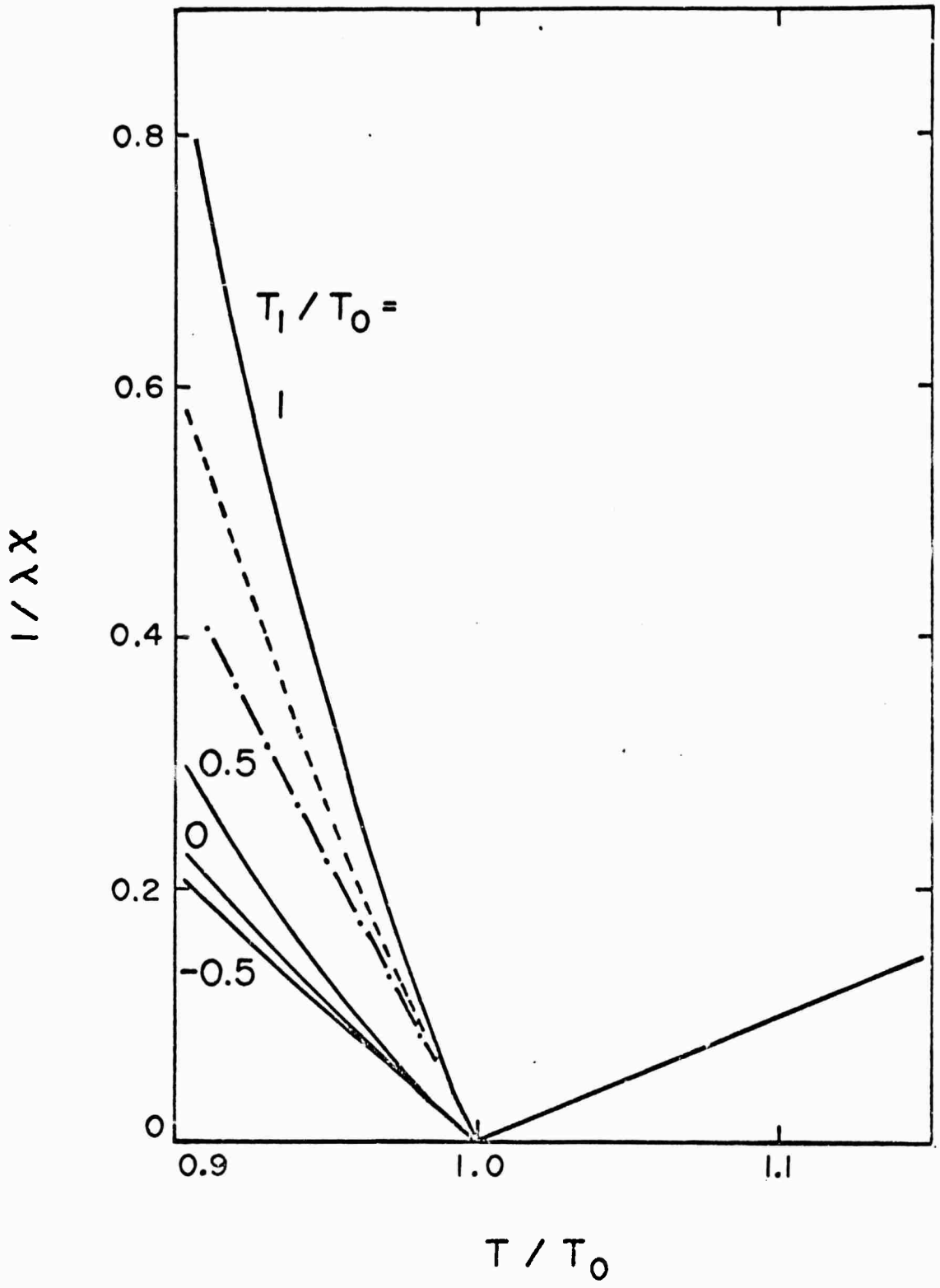

Fig. 10

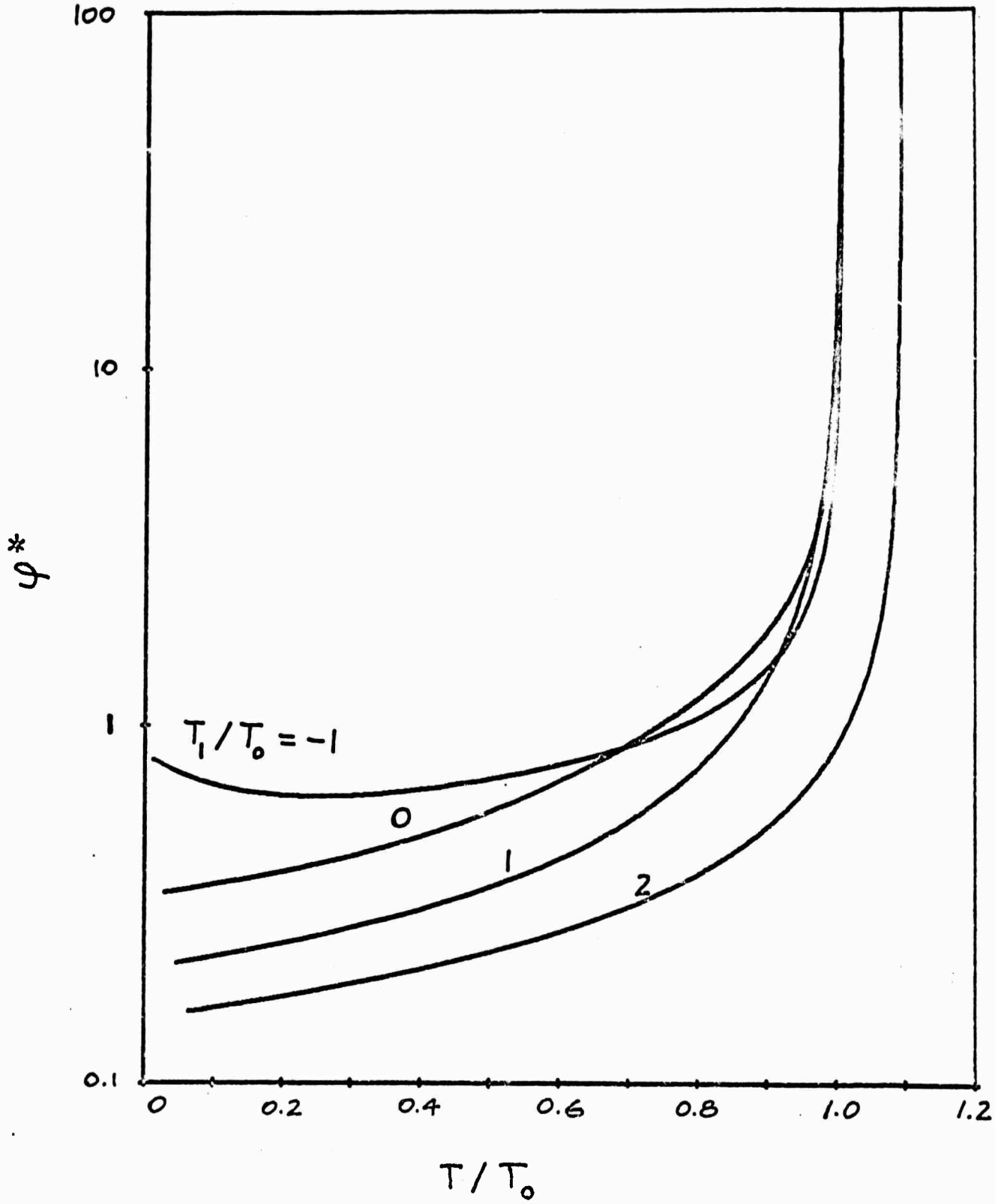

Fig. 11

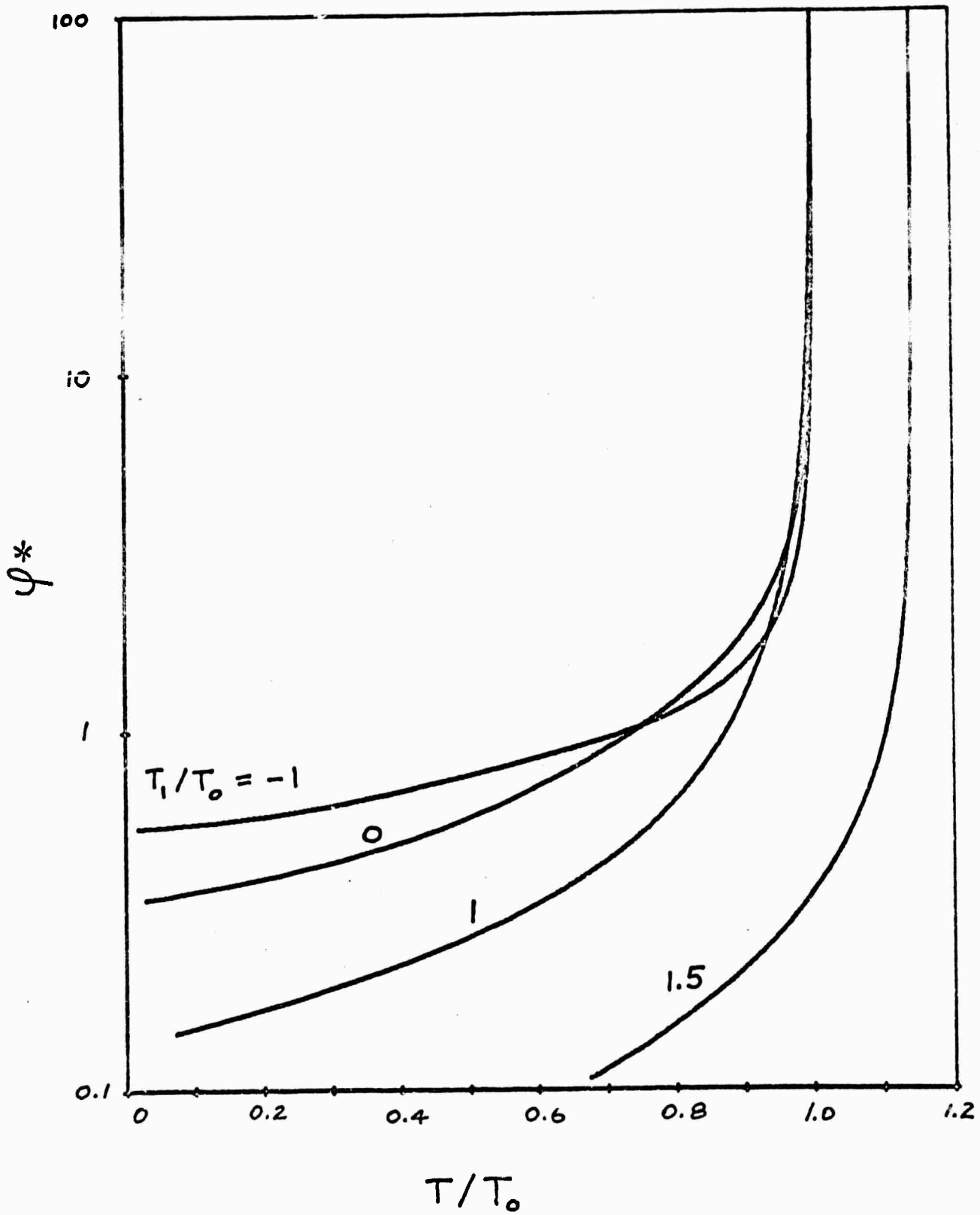

Fig. 12

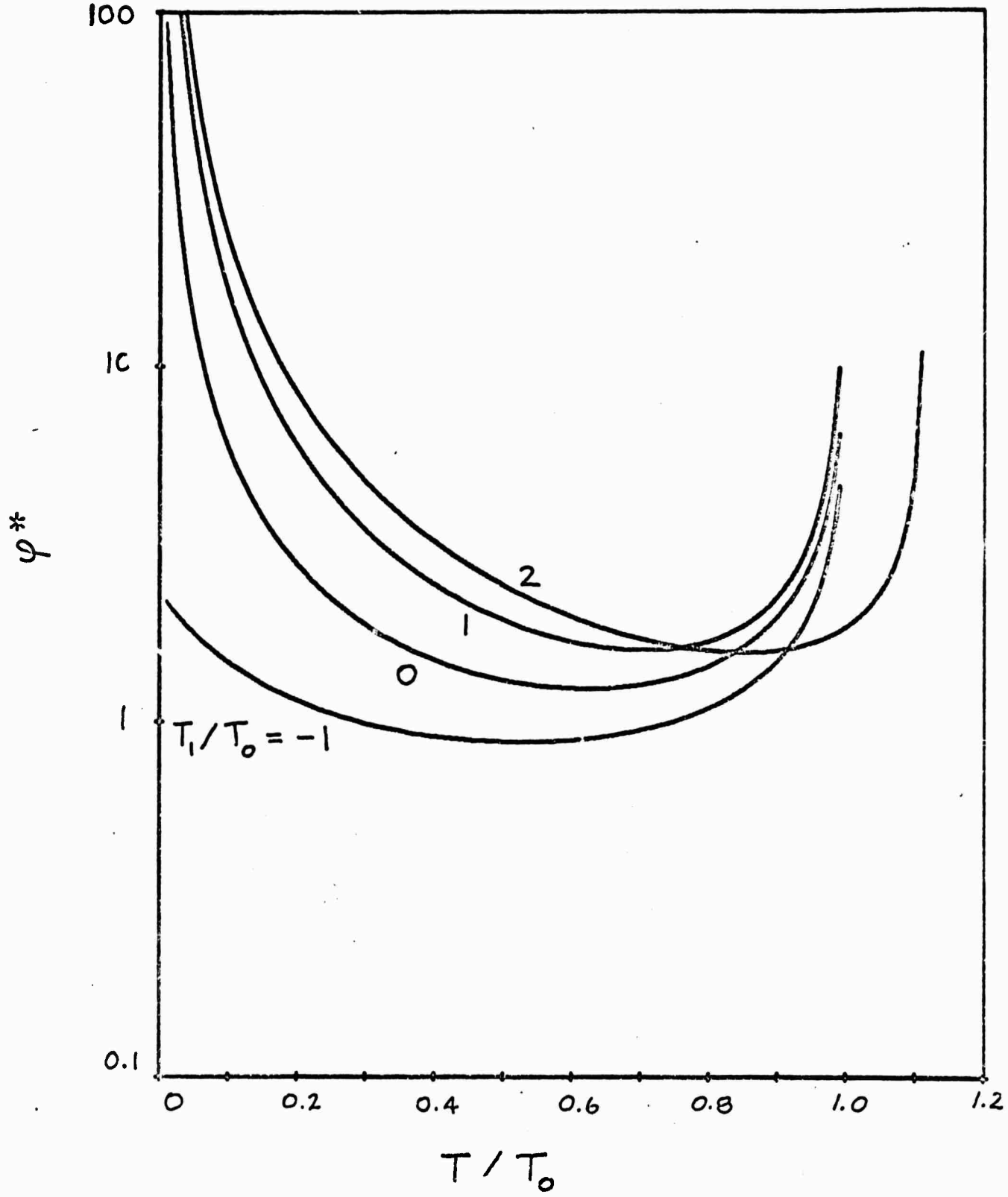

Fig. 13

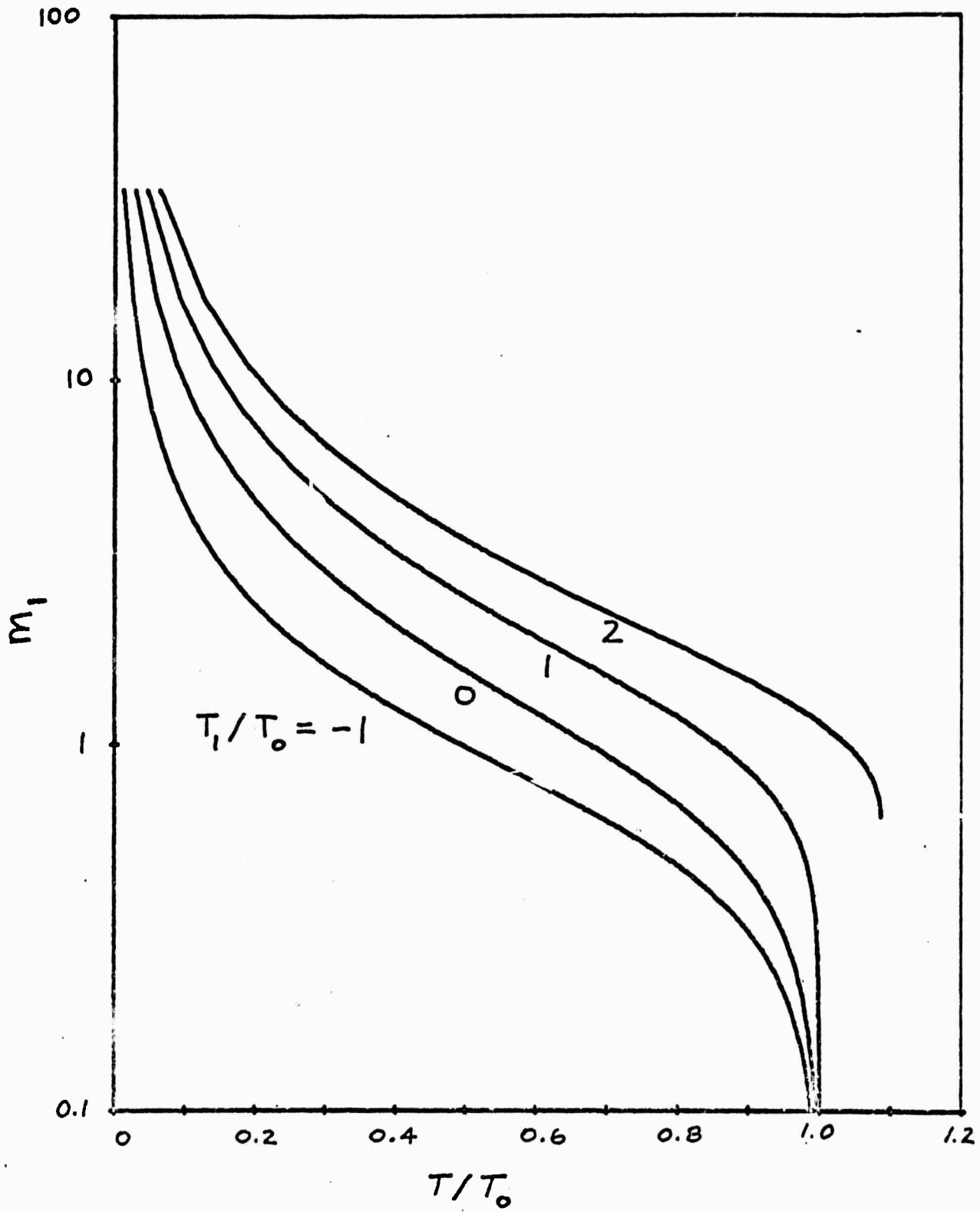

Fig. 14

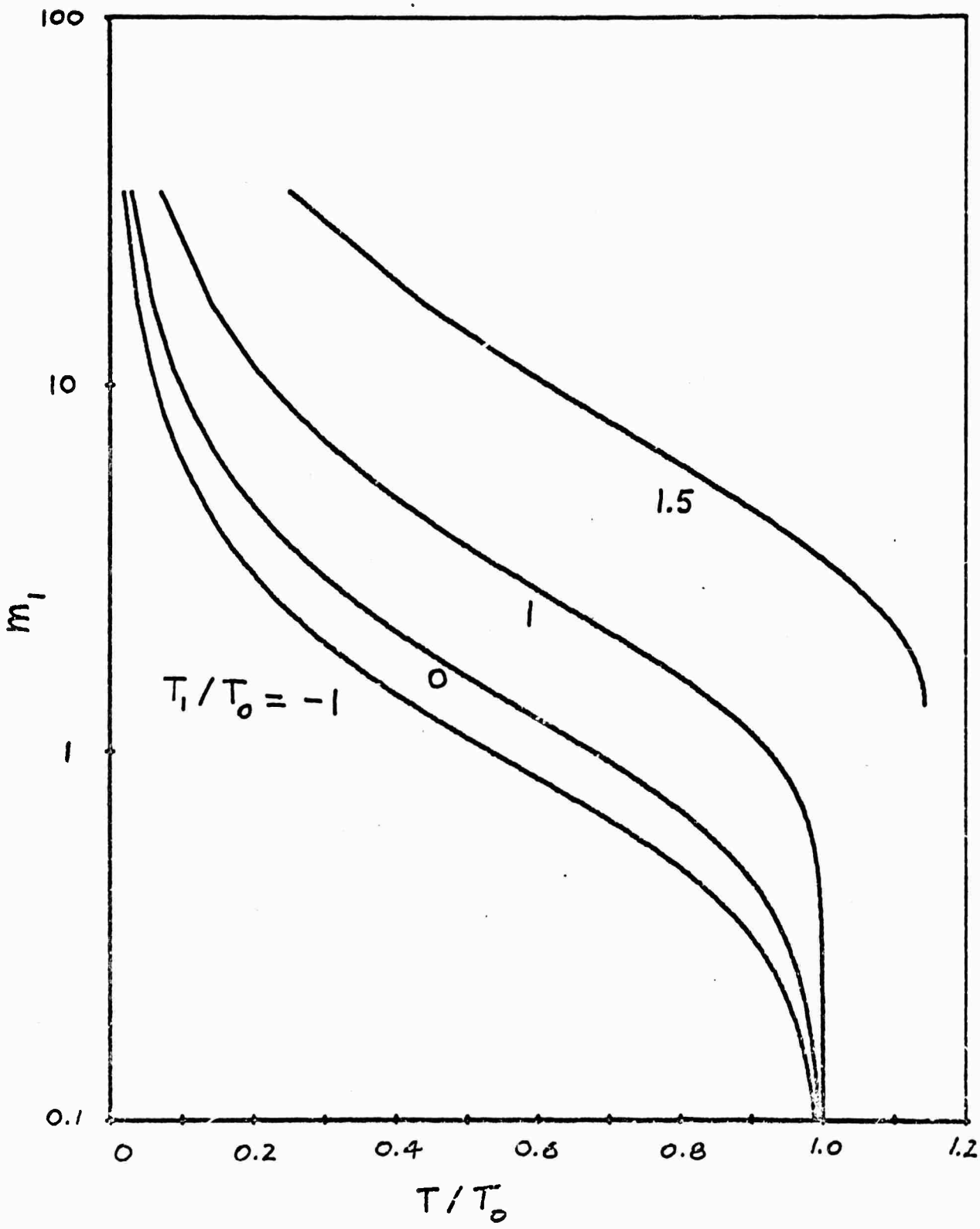

Fig. 15

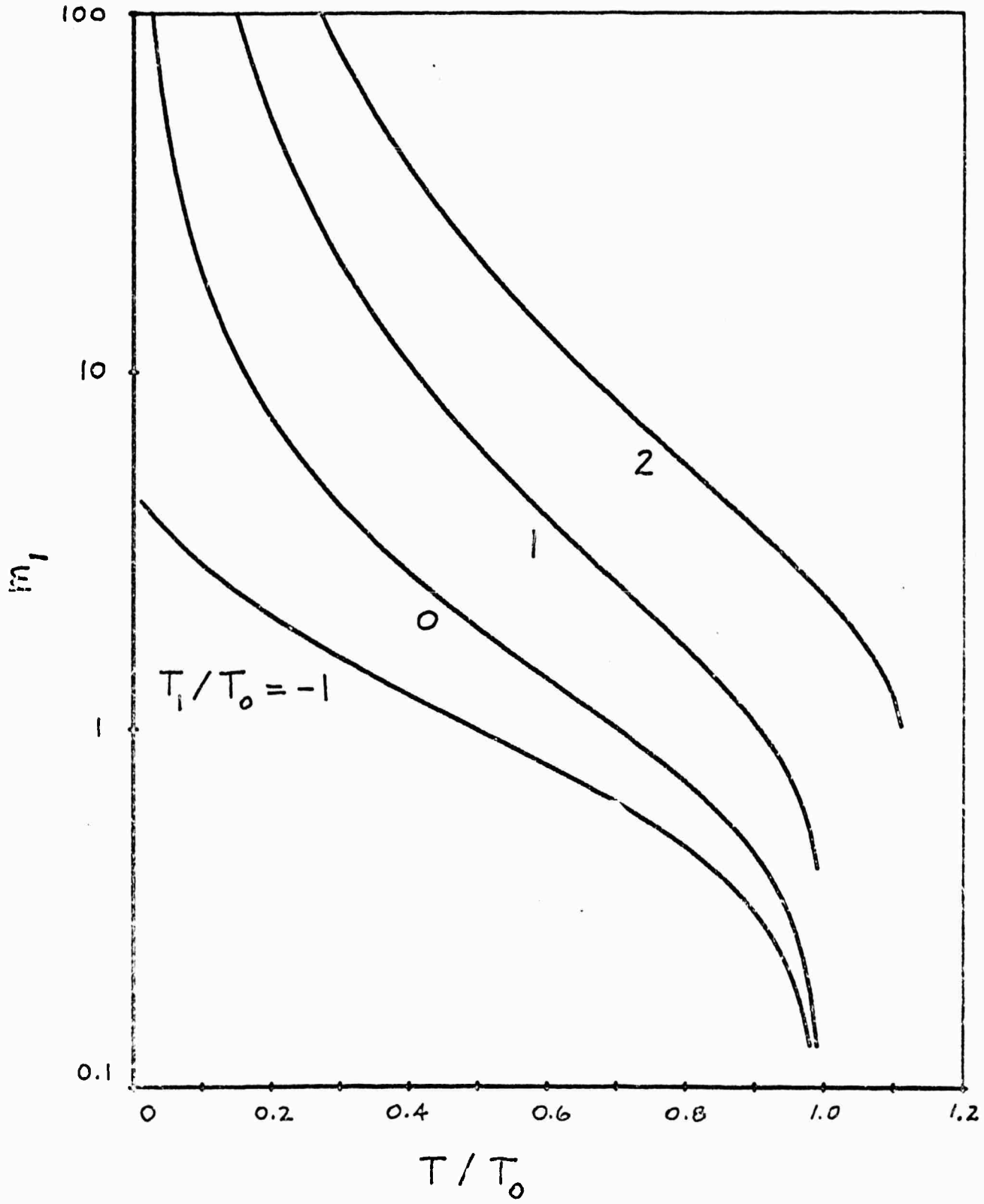

Fig. 16

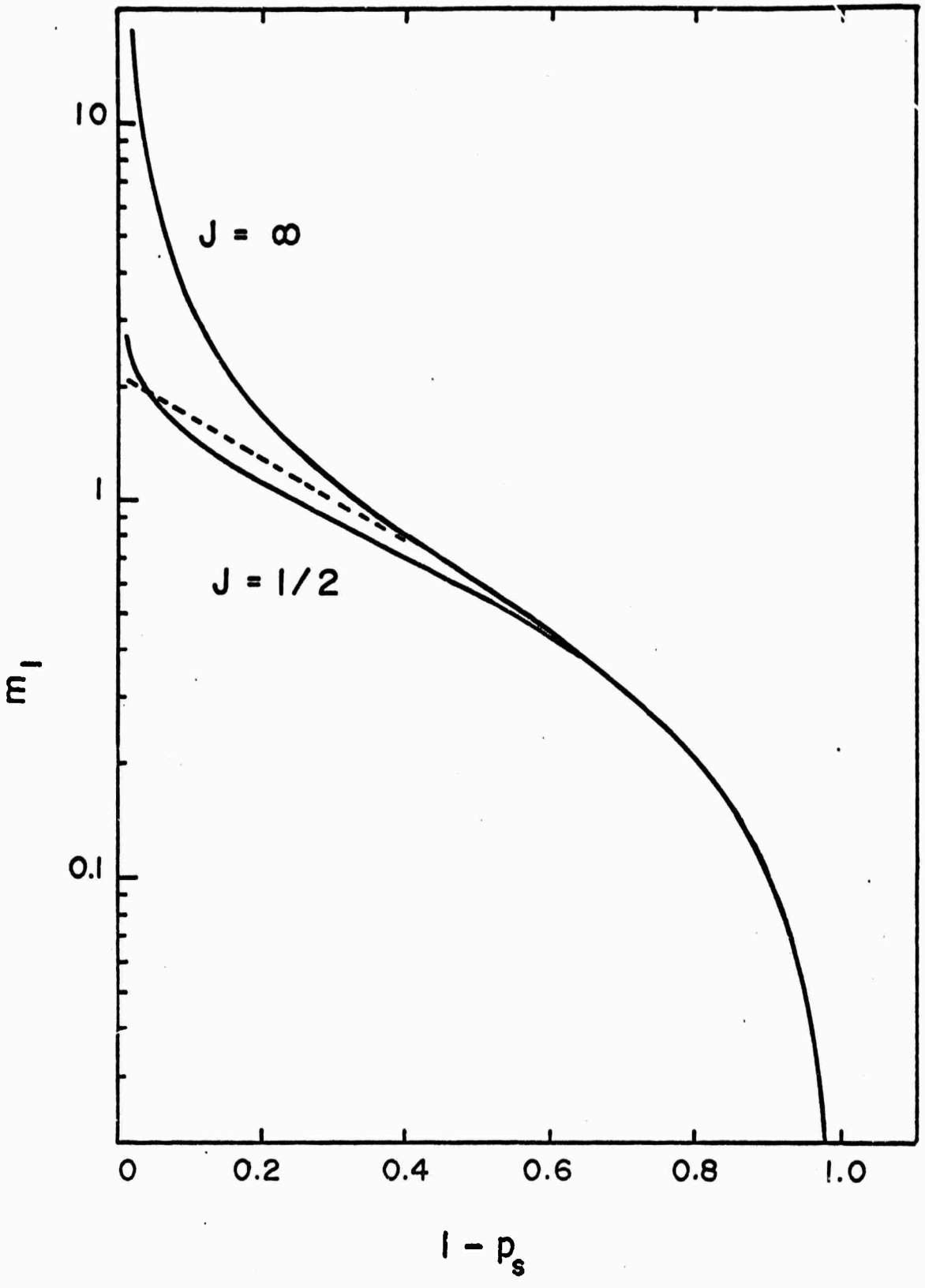

Fig. 17

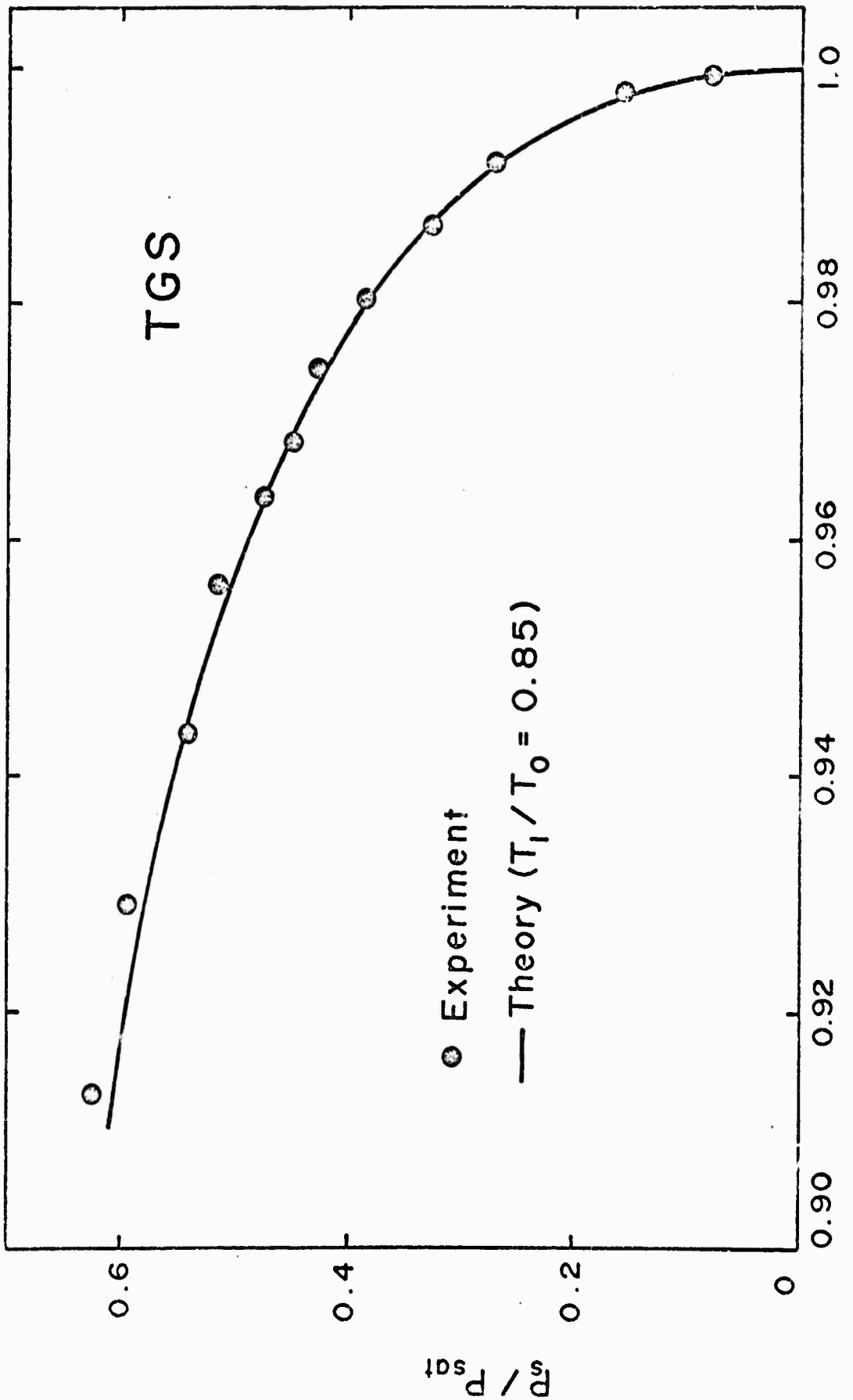
TGS
Experiment
Theory ($T_1 / T_0 = 0.85$)
T / T_0
τ_s / τ_{sat}
0.90
0.92
0.94
0.96
0.98
1.0
0
0.2
0.4
0.6

Fig. 18

DISTRIBUTION LIST

101 Defense Documentation Center
ATTN: DDC-TCA
Cameron Station (Bldg 5)
*012 Alexandria, Virginia 22314

107 Director
National Security Agency
ATTN: TDL
001 Fort George G. Meade, MD
20755

108 Director, Defense Nuclear Agy
ATTN: Technical Library
001 Washington, DC 20305

200 Office of Naval Research
Code 427
001 Arlington, VA 22217

203 Naval Ship Engineering Center
ATTN: Code 6179B
Prince Georges Center Bldg
001 Hyattsville, MD 20782

206 Commander
Naval Electronics Lab Ctr
ATTN: Library
001 San Diego, California
92152

207 Commander
US Naval Ordnance Lab
ATTN: Technical Library
001 White Oak, Silver Spring, MD
20910

210 Commandant, Marine Corps
Hq, US Marine Corps
ATTN: Code AO4C
001 Washington, DC 20380

212 Communications-Electronics Div
Development Center
Marine Corps Develop & Educ Cmd
001 Quantico, Virginia 22134

217 Naval Air Systems Command
Code: AIR-5336
Main Navy Building
001 Washington, DC 20325

301 Rome Air Development Center
ATTN: Documents Library
(TDLD)
001 Griffiss AFB, New York 13440

307 Hq ESD(TRI)
L. G. Hanscom Field
001 Bedford, MA 01730

309 Air Force Avionics Lab
ATTN: AFAL/DOT, STINFO
002 Wright-Patterson AFB, Ohio
45433

310 Recon Central/RSA
AF Avionics Laboratory
001 Wright-Patterson AFB, Ohio
45433

314 Hq, Air Force Systems Cmd
ATTN: DLTE
Andrews AFB
001 Washington, DC 20331

315 Director
Air University Library
ATTN: AUL/LSE-64-285
001 Maxwell AFB, Alabama 36112

319 Air Force Weapons Laboratory
ATTN: Technical Library (SUL)
001 Kirtland AFB, New Mexico
87117

400 HQDA(DAMI-ZA)
002 Washington, DC 20310

405 Ofc, Asst Sec of the Army (R&D)
ATTN: Asst for Research
Room 3-E-379, The Pentagon
001 Washington, DC 20310

408 HQDA(DARD-ARP/Dr R.B. Watson)
001 Washington, DC 20310

409 Commanding General
US Army Materiel Command
ATTN: AMCMA-EE
5001 Eisenhower Ave.
001 Alexandria, Virginia 22333

* DECREASE TO 2 COPIES IF REPORT IS NOT RELEASABLE TO PUBLIC. SEE ECOMM 70-31 FOR TYPES OF REPORTS NOT TO BE SENT TO DDC

415 Commanding General
US Army Materiel Command
ATTN: AMCRD-O
5001 Eisenhower Ave.
001 Alexandria, VA 22333

419 Commanding General
US Army Missile Command
ATTN: AMSMI-RR
(Dr. J. P. Hallowes)
001 Redstone Arsenal, Alabama 35809

421 CG, US Army Missile Command
Redstone Scientific Info Ctr
ATTN: Chief, Document Sect
002 Redstone Arsenal, Alabama 35809

423 Commanding General
US Army Weapons Command
ATTN: AMSWE-REF
001 Rock Island, Illinois 61201

426 Commanding Officer
Vint Hills Farm Station
ATTN: Ch, Systems Engrg Div
Opns Center
001 Warrington, Virginia 22186

430 Commanding Officer
US Army Ordnance School
ATTN: ATSOR-CTD
001 Aberdeen Proving Ground, MD 21005

431 Commander
US Army Intelligence School
ATTN: ATSIT-CTD
001 Fort Huachuca, AZ 85613

433 Hq, US Army Aviation Sys Cmd
ATTN: AMSAV-C-AD
P.O. Box 209
001 St. Louis, Missouri 63166

442 Commanding Officer
Harry Diamond Laboratories
ATTN: Library
001 Washington, D.C. 20438

443 CO, USA Foreign Sci & Tech Ctr
ATTN: AMXST-IS1
220 Seventh St, NE
002 Charlottesville, VA 22901

444 CO, USA Foreign Science Div
ATTN: AMXST CE Division
220 Seventh St, NE
001 Charlottesville, Virginia 22901

448 Commanding Officer
Picatinny Arsenal
ATTN: SMUPA-TVI
001 Dover, N. J. 07801

449 Commanding Officer
Picatinny Arsenal
ATTN: SMUPA-RT-S, Bldg 59
002 Dover, N. J. 07801

451 Commanding Officer
Frankford Arsenal
ATTN: L8400 (Dr. W. McNeill)
001 Philadelphia, PA 19137

462 Commanding Officer
US Army Materials and Mech
Research Center
ATTN: AMXMR-ATL, Tech Lib Br
001 Watertown, Mass. 02172

463 President
US Army Artillery Board
001 Fort Sill, Oklahoma 73503

464 Commanding Officer
Aberdeen Proving Ground
ATTN: Tech Library, Bldg 313
002 Aberdeen Proving Gr, MD 21005

465 Commanding Officer
Aberdeen Proving Ground
ATTN: STEAP-TL
001 Aberdeen Proving Gr, MD 21005

480 Commanding Officer
USASA Test and Evaluation Cen
001 Fort Huachuca, Arizona 85613

483 US Army Research Office-Durham
ATTN: CRDARD-IP
Box CM, Duke Station
001 Durham, N. C. 27706

484 US Army Research Ofc-Durham
ATTN: Dr. Robert J. Lontz
Box CM, Duke Station
001 Durham, North Carolina 27706

486 Commanding Officer
USA Mobility Eqpt R&D Cen
ATTN: Tech Doc Cen, Bldg 315
002 Fort Belvoir, Virginia 22060

488 USA Security Agency
ATTN: IARD
Arlington Hall Sta, Bldg 420
001 Arlington, Virginia 22212

489 Commanding General
US Army Tank-Automotive Command
ATTN: AMSTA-RH-FL
001 Warren, Michigan 48090

492 Commandant
US Army Air Defense School
ATTN: C&S Dept, MSL Sci Div
001 Fort Bliss, Texas 79916

493 Director
USA Engr Waterways Exper Sta
ATTN: Research Center Library
002 Vicksburg, Mississippi 39180

495 CG, Deseret Test Center
ATTN: STEPD-TT-ME(S) Met Div
Bldg 103, Soldiers Circle
001 Fort Douglas, Utah 84113

500 Commanding Officer
Yuma Proving Ground
ATTN: STEYP-AD (Tech Lib)
001 Yuma, Arizona 85364

501 Commanding Officer
US Army Arctic Test Center
002 APO, Seattle 98733

502 CO, USA Tropic Test Center
ATTN: STETC-MO-A (Tech Lib)
Drawer 942
001 Fort Clayton, Canal Zone 09827

503 Director
US Army Adv Matl Concepts Agcy
ATTN: AMXAM
001 Washington, D. C. 20315

504 Commanding General
US Army Materiel Command
ATTN: AMCRD-R
5001 Eisenhower Ave.
001 Alexandria, VA 22333

512 Commanding Officer
USACDC Armor Agency, ATTN: ATSAR-CTD
001 Fort Knox, Kentucky 40121

516 Commandant
US Army Field Artillery School
ATTN: Target Acquisition Dept
002 Fort Sill, Oklahoma 73503

517 Commanding General
US Army Missile Command
ATTN: AMSMI-RFG (Mr N. Bell)
001 Redstone Arsenal, Ala. 35809

518 Commanding Officer
Harry Diamond Laboratories
ATTN: AMXDO-RCB (Mr. Nemarich)
001 Washington, D. C. 20438

596 Commanding Officer
US Army Southeastern Signal School
ATTN: ATSN-CTD-MS
001 Fort Gordon, GA 30905

598 Commanding Officer
USA Satellite Comm Agency
ATTN: AMCPM-SC-3
001 Fort Monmouth, N. J. 07703

599 Tri-Tac Office
ATTN: CSS (Dr. Pritchard)
001 Fort Monmouth, N. J. 07703

607 Commanding General
USA Tank-Automotive Command
ATTN: AMSTA-Z, Dr. J. Parks
001 Warren, Michigan 48090

610 Director
Night Vision Lab (USAECOM)
ATTN: AMSEL-NV-D
001 Fort Belvoir, Virginia 22060

614 Chief
Ofc of Missile Electronic Warfare
Electronic Warfare Lab, ECOM
001 White Sands Missile Range, NM
88002

616 CG, USA Electronics Command
ATTN: AMSEL-PP/P-IED
(Mr. C. Mogavero)
225 South 18th Street
001 Philadelphia, PA. 19103

617 Chief, Intel Materiel Dev & Support
Ofc, Electronic Warfare Lab, (ECOM)
001 Fort Meade, MD 20755

680 Commanding General
US Army Electronics Command
000 Fort Monmouth, N. J. 07703

1AMSEL-NV-D 1AMSEL-RD
1AMSEL-NL-D
1AMSFL-WL-D 1AMSEL-TL-D
1AMSEL-VL-D
1AMSEL-CT-D
1AMSEL-BL-D
1AMSEL-TL-DT
6 AMSEL-TL-ES
(Ofc of Record)

{ ECOM in-house reports only

1AMSEL-TE

2AMSEL-MS-TI
1AMSEL-GG-TD
1AMSEL-EN
1AMSEL-PA
1USMC-LNO
1 AMSEL-PP-C-ES-I

* Or number specified in contract Add COTR's mail symbol

703 NASA Sci & Tech Info Facility
ATTN: Acquisitions Br(S-AK/DL)
P.O. Box 33
002 College Park, Maryland 20740

705 Advisory Gp on Electron Devices
201 Varick St. 9th Floor
002 New York, New York 10014

706 Advisory Gp on Electron Devices
ATTN: Secy, Sp Gr on Opt Masers
201 Varick Street
002 New York, New York 10014

708 Ballistic Msl Radiation Anal Cen
Univ of Mich., Willow Run Lab
Institute of Science & Tech
001 PO Box 618, Ann Arbor, Michigan
48107

711 Metals and Ceramics Inf Center
Battelle
505 King Avenue
001 Columbus, Ohio 43201

712 Elec Properties Info Center
Hughes Aircraft Company
Centinela and Teale Streets
001 Culver City, California 90230

715 Plastics Tech Eval Center
Picatinny Arsenal, Bldg 3401
001 Dover, N. J. 07801

717 Reliability Analysis Center
Rome Air Development Center
ATTN: J.M. Schramp/RCRM
001 Griffiss AFB, New York 13440

718 Remote Area Confligt Info Ctr
Battelle Memorial Institute
505 King Avenue
001 Columbus, Ohio 43201

719 Shock and Vibration Info Center
Naval Research Lab (Code 6020)
001 Washington, D. C. 20390

720 Thermophysical Properties Res Ctr
Purdue Univ., Research Park
2595 Yeager Road
001 Lafayette, Indiana 47906

721 Vela Seismic Info Center
University of Michigan
Box 618
003 Ann Arbor, Michigan 48107

Department of Electrical Engineering
ATTN: Dr. A. van der Ziel
University of Minnesota
001 Minneapolis, MN 55455

Dr. George Hellmeier
Director, Advanced Research
Project Agency
1400 Wilson Blvd.
002 Arlington, VA 22209

C Commander
US Army Combined Arms Combat
Developments Activity
ATTN: ATCAIC
001 Fort Leavenworth, KS 66027

Commander
US Army Training & Doctrine Command
ATTN: ATCD-CI
001 Fort Monroe, VA 23651

Director
Naval Research Laboratory
CODE 2627
001 Washington, DC 20390

Commander
US Army R&D Group
(Far East)
003 APO, San Francisco, CA 96343

Commandant
US Army Engineer School
ATTN: ATSEN-CTD
001 Fort Belvoir, VA 22060

Commanding General
US Army Materiel Command
ATTN: AMCRD-TP (Dr. B. Zarwyn)
5001 Eisenhower Ave.
001 Alexandria, VA 22333

Institute of Science & Tech
The University of Michigan
P.O. Box 618 (IRIA Library)
001 Ann Arbor, MI 48107

Director, Night Vision Laboratory
US Army Electronics Command
ATTN: AMSEL-NV-FIR (Dr. R. Ennulat)
001 Fort Belvoir, VA 22060

Director, Night Vision Laboratory
US Army Electronics Command
ATTN: AMSEL-NV-D (Mr. Edward C. Walker)
001 Fort Belvoir, VA 22060